Theses and Dissertations

2017

# Investigation on the Surface Plasmon Dispersion Engineering with TiN-Based Structures

Yiming Zhong
*Lehigh University*

# Investigation on the Surface Plasmon Dispersion Engineering with TiN-Based Structures

by

Yiming Zhong

A Thesis

Presented to the Graduate and Research Committee

of Lehigh University

in Candidacy for the Degree of

Master of Science

in

Electrical Engineering

Lehigh University

May 2017

This thesis is accepted and approved in partial fulfillment of the requirements for

the Master of Science.

Date: <u>May 3rd , 2017</u>

<br>

_____

Prof. Nelson Tansu,

M.S. Advisor

<br>

_____

Prof. Svetlana Tatic-Lucic,

ECE Interim Department Chair

# Acknowledgement

With several months of work, my Master thesis has come out and I believe it is the reflection of the efforts during my Master study at Lehigh. The completion of this work would not be possible without the great support from many people in my life, and I would like to thank the following people especially for their great support.

First and foremost, I would sincerely express my great gratitude to my advisor, Prof. Nelson Tansu, on both his academic guidance for my research and the living philosophy for my life. It is my great pleasure to work in Prof. Tansu' s group at Center for Photonics and Nanoelectronics (CPN) at Lehigh during these two years, which made me gain a lot of knowledge and develop my serious professional attitude in the research. Prof. Tansu's profound knowledge and inspiration in scientific research has deeply influenced me, and I believe I will benefit a lot from what I have learned from him in my future career.

My gratitude also goes to my mentor, Ioannis Fragkos, for his great help and assistance while working with me. His excellent professional ability and valuable advices helped me a lot with my work.

I would also like to express my appreciation to my lab mates who have given me great assistance and encouragement during the time I worked in the lab: Prof. Chee-Keong Tan (Clarkson University), Wei Sun, Liangyue Yan, Damir Borovac, Austin M. Slosberg, Xiongliang Wei, Guosong Zeng, Eric T. Reid, Justin C. Goodrich, Onoriode Ogidi-Ekoko, and Hanlin Fu. In particular, I would like to thank Liangyue Yan, who generously gave me a lot of help on both of my study and living perspective.

I would like to thank two of my friends: Dan Zhu, and Yao Sun for providing their indispensable companion and encouragement in my life.

Last, but most importantly, I would express my deepest gratitude to my mother, Caiping Liu, and my father, Huaping Zhong, for their endless love and support in my life. They are the role models in my life for their great dedication to the family, excellent contribution to the career, and positive attitude in the life. The support and education I received from them built the initial foundation and motivation of my pursuit of study. My parents' great input to my life made me become a person that I wish to be.

# Table of Contents

# List of Figures and Table

# Abstract

In this thesis, we investigate the efficiency enhancement of surface plasmon (SP) coupling to the InGaN/ GaN QWs LED based on the strongly localized optical field and highly enhanced photon density of states near the SP frequency ($\omega_{sp}$) according to Purcell enhancement factor. Based on the Purcell effect, when the emission frequency approaches the surface plasmon frequency coupled to the active region, the energy coupled to the SP will notably increase and hence IQE will be strongly enhanced.

In order to achieve the desirable long-wavelength emission and enhance the radiative efficiency for InGaN QWs LED, TiN and Au are selected as the appropriate materials for allowing the design of the surface plasmon frequency in the long-wavelength spectral regime (green-red). Such optimum design for engineering the surface plasmon frequency of the nano-metallic structures will result in enhanced radiation recombination rate from the active region.

In this thesis, we investigate both single and double metallic layers structure to get the optimized model for Purcell enhancement in long-wavelength range. The effect of the metallic layer thicknesses has been exhibited in the computational studies. The Au and TiN single-layer structures can achieve the strong Purcell factor of ~1000 times and ~550 times in green and amber regime, respectively. The tunability of the SP frequency can be achieved by using the TiN/Au double-metallic layer structures for achieving optimized design to cover the peak Purcell factor ~ 500 times across the range of the surface plasmon frequencies of Au and TiN. The effect of different spacer separation between the InGaN QWs and metallic layer is also investigated. The variation of the spacer thickness affects the coupling efficiency, and this increased thickness also reduces the Purcell enhancement factor and decreases the surface plasmon frequency.

# Chapter 1: Introduction

## 1.1. Challenges of Conventional InGaN QW LEDs

GaN based light emitting diodes (LEDs) are currently the subject of extensive research interest and has been widely commercialized due to the widespread applications in the areas of photonics, including solid state lighting [1]-[2], LCD backlighting [3], full-color displays [4], power electronics [5], thermoelectricity [6], and solar cells [7]. Nowadays for the high-efficiency, high-output, and energy-saving purposes, white- and full-color lighting technology require a monolithic device composed of red, green and blue GaN based LEDs.
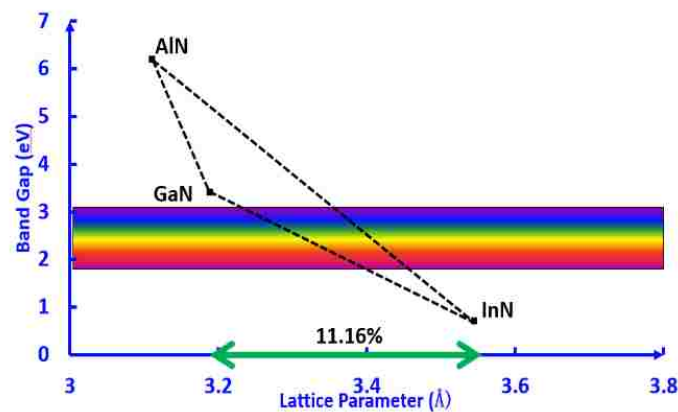


**Figure 0-1.** Bandgap and lattice constant mismatch of GaN and InN.

In the past years, the InGaN alloy has been used as the active layer in GaN light emitting diodes radiating in blue and green spectral regimes. The InGaN alloy allows the emission from the ultraviolet up to entire visible spectral regimes, and the engineering of the $In_xGa_{1-x}N$ QWs with higher In-content have the potential to access into the important "red emission" spectral regime. However, the strain misfit

dislocation density from lattice mismatch of InGaN (3.545 Å) and GaN (3.189Å)

results in higher density of nano-scale In-rich clusters through spinodal decomposition

and other mechanisms [8]-[9]. Thus, high In-incorporation in growing InGaN/GaN QW

for efficient long-wavelength light emission is usually difficult, and the poor material

quality will lead to the low internal quantum efficiency (IQE) of InGaN QWs in the

long-wavelength regime [10]. The challenges in achieving high efficiency InGaN-

based quantum well light-emitting diodes (LEDs) in the long-wavelength (green-red)

spectral regimes are attributed to the low radiative recombination rate and poor material

quality from this active region alloy containing high In-content. Hence, these issues

will lead to the low IQE of InGaN QWs LEDs operating at longer wavelength.
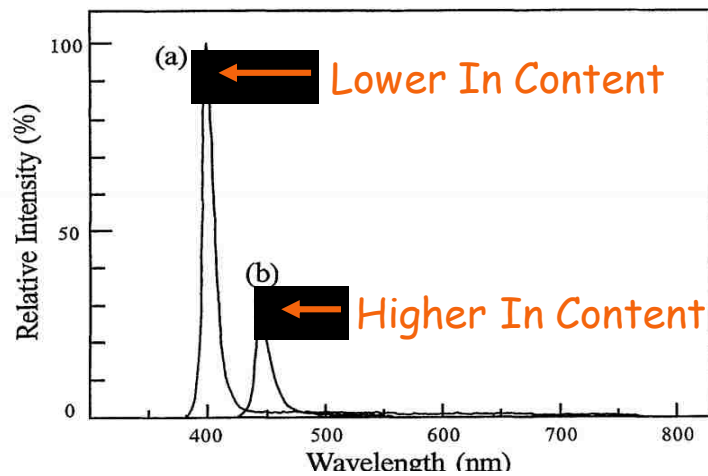


**Figure 0-2.** Room temperature PL measurement of InGaN film grown on GaN under same growth conditions except for the InGaN growth temperature (a) 830°C, In=0.14, (b) 780°C, In=0.24 [15].

Another important limitation is related to the charge separation induced by the

large internal field in the InGaN QW. This large internal field is attributed to the strong

spontaneous and piezoelectric fields in the InGaN/GaN QWs [11]-[12]. As the InGaN

and GaN layers have different polarization properties, this results in the built-in field

within the active region. Additionally, as there is a p-i-n junction, it will also have a built-in field in the QWs. Considering those fields altogether, there will be a net field from p-type layer to n-type layer, which mainly produced by the polarization field. With such an internal field, there will be a potential tilt in the QW, which results in the charge separation of the electronics and holes in the active region. Such charge separation will result in the reduced internal quantum efficiency in the long-wavelength range, and consequently affect the overall efficiency of LED.
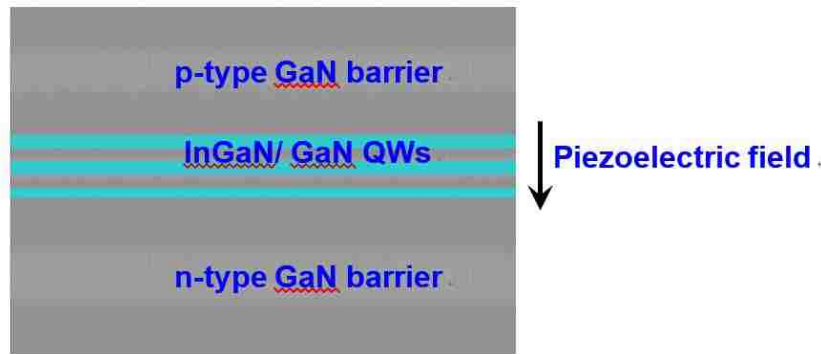


**Figure 0-3.** Structure of InGaN/ GaN QW LED

## 1.2.    Motivation

To solve the charge separation issue, several methods with improved electron-hole wave function overlap ($\Gamma_{eh}$) have been proposed [13]–[19], such as the staggered InGaN QW, type-II InGaN/GaNAs QW, strain-compensated InGaN-AlGaN QW, InGaN-delta-InN QW. The proposed LED works well on red spectrum of visible light emitting range, however it suffers from lower efficiency comparing to blue and green emission. To solve the low efficiency problem, we propose to use surface plasmon (SP) coupled LED which works based on the strongly localized optical field and highly enhanced photon density of states near the surface plasmon frequency ($\omega_{sp}$) according

4

to Purcell factor [20]. Purcell effect is the basic idea of emission enhancement of surface plasmon. When you put a radiating dipole near the metal structure in the resonance cavity, the emission efficiency will be improved and enhanced. Due to Purcell effect, when $\omega_{sp}$ overlaps with the emission frequency of the quantum wells, the energy coupled to the surface plasmon will notably increases, which enhances the LED efficiency at long-wavelength emission.

Recently the approaches based on metallo-dielectric stacks structure [21] and double-metallic layers structure [22] on InGaN QW-based LEDs had been reported to tune the surface plasmon frequency and enhance the radiation rate of nearby active region. The use of surface plasmon coupled active region to increase the photon density of states has been demonstrated in the blue and green spectral regime in many reports, especially the strong enhancement of Ag layer and Au/Ag double layers for blue and green spectral regimes. In this work, the tuning of the SP frequency over a wide frequency range while maintaining a large Purcell factor by using SP will be presented.

## 1.3. Thesis organization

Chapter 1 introduces the background and motivation of using surface plasmon to enhance the efficiency of InGaN QW LEDs in the long-wavelength range. Chapter 2 illustrates the basic concept and the effect of surface plasmon coupled to InGaN QWs for the enhancement of IQE. In Chapter 3, the general formulation for the calculation of SP modes in the planar structures containing multilayers. Chapter 4 explores the optical properties of different materials to find the proper and applicable plasmonic

5

materials with $\omega_{sp}$ in the range of long-wavelength emission to couple to the InGaN QWs. This chapter also exhibits the simulation results of the dispersive properties and Purcell factor for different SP structure with single or double metallic layers, and hence find the optimized design for SP model which is appropriate and compatible for achieving strong Purcell factors in SP coupling. Chapter 4 also analyzes the factors that affect SP structure by using different configuration of thicknesses of metallic layer and GaN spacer. The summary and future work are included in Chapter 5.

**References for Chapter 1**

1.  Nelson Tansu, Hongping Zhao, Guangyu Liu, Xiao-Hang Li, Jing Zhang, Hua Tong, and Yik-Khoon Ee. "III-Nitride Photonics." *IEEE Photonics Journal,* 2, 241-248 (2010).

2.  Daniel A. Steigerwald, Jerome C. Bhat, Dave Collins, Robert M. Fletcher, Mari Ochiai Holcomb, Michael J. Ludowise, Member, IEEE, Paul S. Martin, and Serge L. Rudaz. "Illumination with solid state lighting technology." *IEEE Journal of Selected Topics in Quantum Electronics*, 8, 310-320 (2002).

3.  Anandan, Munisamy. "Progress of LED backlights for LCDs." *Journal of the Society for Information Display,* 16, 287–310 (2008).

4.  Okamoto, Koichi. "Surface plasmon enhanced solid-state light-emitting devices." In Nanoscale Photonics and Optoelectronics, pp. 27-46. Springer New York (2010).

5.  Sato, Yuichi, N. Takahashi, and S. Sato. "Full-Color Fluorescent Display Devices Using a Near-UV Light-Emitting Diode." *Japanese Journal of Applied Physics* 35.7A, L838-L839 (1996).

6.  S.J. Pearton, F. Ren, A.P. Zhang, G. Dang, X.A. Cao, K.P. Lee, H. Cho, B.P. Gila, J.W. Johnson, C. Monier, C.R. Abernathy, J. Han, A.G. Baca, J.-I. Chyi, C.-M. Lee, T.-E. Nee, C.-C. Chuo, S.N.G. Chu. "GaN electronics for high power, high temperature applications." *Materials Science & Engineering B* 82.1, 227-231 (2000).

7.  B. N. Pantha, R. Dahal, J. Li, J. Y. Lin, and H. X. Jiang. "Thermoelectric properties of InxGa1−xN alloys."*Applied Physics Letters* 92.4:42-82 (2008).

8.  R. M. Farrell, C. J. Neufeld, S. C. Cruz, J. R. Lang, M. Iza, S. Keller, S. Nakamura, S. P. DenBaars, U. K. Mishra, and J. S. Speck. "High quantum efficiency InGaN/GaN multiple quantum well solar cells with spectral response extending out to 520 nm." *Applied Physics Letters* 98.20, 160 (2011).

9.  Schulz, Heinz, and K. H. Thiemann. "Crystal structure refinement of AlN and GaN." *Solid State Communications* 23.11, 815-819 (1977).

10. C. C. Yang, Shih-Wei Feng, Yen-Sheng Lin, Yung-Chen Cheng, Chi-Chih Liao, Chin-Yi Tsai, and Kung-Jeng Ma, Jen-Inn Chyi. "Indium segregation in InGaN/GaN quantum well structures." *Proc Spie* 4280, 20-26 (2001).

11. Nakamura, Shuji, and T. Mukai. "High-Quality InGaN Films Grown on GaN Films." *Japanese Journal of Applied Physics*31.10B, L1457-L1459 (1992).

12. Christian WETZEL, Satoshi KAMIYAMA, Hiroshi AMANO and Isamu AKASAKI. "Optical Absorption in Polarized Ga1-xInxN/GaN Quantum Wells." *Japanese Journal of Applied Physics* 41.1, 11-14 (2002).

13. Ronald A. Arif, Yik-Khoon Ee, and Nelson Tansu. "Polarization engineering via staggered InGaN quantum wells for radiative efficiency enhancement of light emitting

diodes." *Applied Physics Letters* 91.9, 091110 (2007).

14. Koichi Okamoto, Isamu Niki, Axel SchererYukio Narukawa and Takashi MukaiYoichi Kawakami. "Surface plasmon enhanced spontaneous emission rate of InGaN∕GaN quantum wells probed by time-resolved photoluminescence spectroscopy." *Applied Physics Letters*87.7, 1687 (2005).

15. Nakamura, Shuji, and T. Mukai. "High-Quality InGaN Films Grown on GaN Films." *Japanese Journal of Applied Physics*31.10B, L1457-L1459 (1992).

16. Robert M. Farrell, Daniel F. Feezell, Mathew C. Schmidt, Daniel A. Haeger, Kathryn M. Kelchner, Kenji ISO, Hisashi Yamada, Makoto Sasito, Kenji Fujito, Daniel A. Cohen, James S. Speck, Steven P. Denbaars, and Shuji Nakamura. "Continuous-wave Operation of AlGaN-cladding-free Nonpolar m-Plane InGaN/GaN Laser Diodes." *Japanese Journal of Applied Physics* 46.29-32, L761-L763 (2007).

17. H.P. Zhao, G.Y. Liu, X.-H. Li, R.A. Arif, G.S. Huang, J.D. Poplawsky, S. Tafon Penn, V. Dierolf, N. Tansu. "Design and characteristics of staggered InGaN quantum-well light-emitting diodes in the green spectral regime." *Iet Optoelectronics* 3.6, 283-295 (2009).

18. Zhao, Hongping, and N. Tansu. "Optical gain characteristics of staggered InGaN quantum wells lasers." *Journal of Applied Physics*107.11, 113110 (2010).

19. Seoung-Hwan Park, Yong-Tae Moon, Jeong Sik Lee, Ho Ki Kwon, Joong Seo Park and Doyeol Ahn. "Spontaneous emission rate of green strain-compensated InGaN/InGaN LEDs using InGaN substrate." *Physica Status Solidi* 208.1, 195–198 (2011).

20. E. M. Purcell, "Proceedings of the American Physical Society." *Phys Rev* 69.3-4, 133-133 (1946).

21. John Henson, Anirban Bhattacharyya, Theodore D. Moustakas and Roberto Paiella. "Controlling the recombination rate of semiconductor active layers via coupling to dispersion-engineered surface plasmons." *Journal of the Optical Society of America B* 25.8, 1328-1335 (2008).

22. Hongping Zhao, Jing Zhang, Guangyu Liu, and Nelson Tansu. "Surface plasmon dispersion engineering via double-metallic Au/Ag layers for III-nitride based light-emitting diodes." *Applied Physics Letters* 98.15, 236 (2011).

# Chapter 2: Theory of Surface Plasmon Polariton

## 2.1.    Basic Concept of Surface Plasmon Polariton

The phenomenon of radiative efficiency enhancement via using metal film has been known for many years since 1974 [1]-[2]. For InGaN QW, the coupling for the spontaneous emission from QW into the SP mode on silver thin film method was initially demonstrated through the observation of spectrally sharp photoluminescence dip in 1999 by I. Gontijo, et al. [5]. Then it has been used as a method to enhance the efficiency of InGaN QW LEDs by K. Okamoto, et al. in 2004 [6]. Conventionally, noble metals especially gold and silver are used as plasmonic materials for their strong enhancement for efficiency. The recombination rate in InGaN/GaN QWs could be significantly enhanced from the metal surface, and increased absorption of light at the SP frequency has been demonstrated.

The plasmon is the collective oscillation of conducting electron gas responding to an electric field, in a metal, and a special phenomenon of plasma oscillation mode is called surface plasmon (SP). Surface plasmon exists at an interface between a metal, which has a dielectric function $\varepsilon_m = \varepsilon'_m + i\varepsilon''_m$, and a dielectric or semiconductor material, which has a positive real dielectric constant $\varepsilon_d$. If the collective motion oscillation of electrons is excited on the surface, it can produce the surface plasmon resonance (SPR). Surface plasmon resonance occurs when a resonance of the charge density wave matches the frequency of the applied field. The bulk oscillation of electrons and an electromagnetic wave outside of the metal will couple with the other, which results in the remaining surface wave.
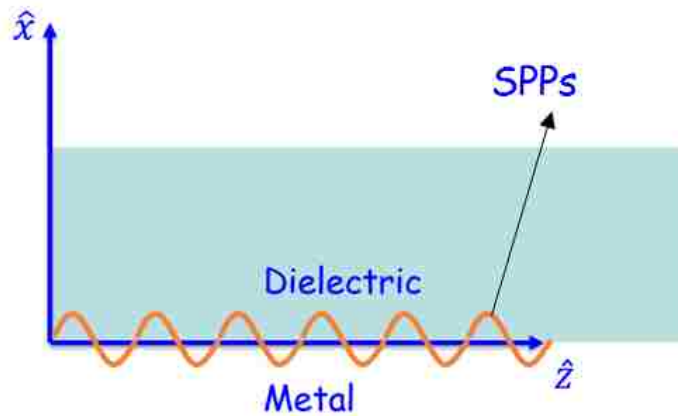
**Figure 0-1.** Geometry for SPP propagation at a single interface between a metal and a dielectric.

Surface plasmon polaritons (SPPs) is a kind of surface wave of which the mode is confined at the interface between metal and dielectric. SPPs couple the electromagnetic wave to oscillations of conducting electron plasma, and it only exists for TM mode. They propagate in the longitudinal direction, which is in the dielectric-metal interface, and evanescently confined in the perpendicular direction on both sides of the interface. The evanescent wave is a near-field wave with an intensity that exhibits the exponential decay without absorption as a function of distance from the boundary at where the wave was formed, which confines the energy in a small area.
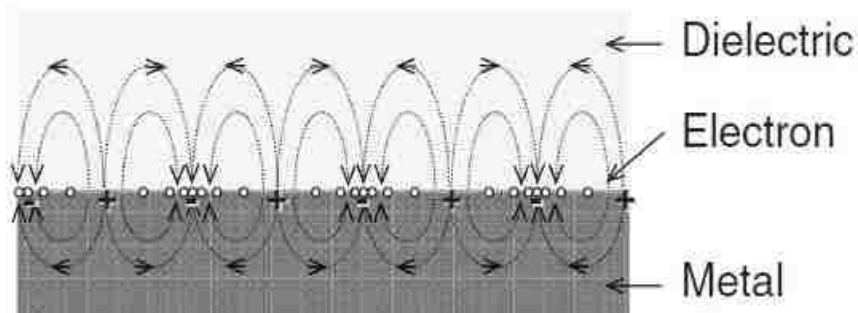


**Figure 0-2.** Schematic Diagram of the surface plasmon and surface plasmon polariton generated at the metal/ dielectric interface [4]

In order to couple energy from a QW to the surface plasmon mode, the plasmonic material plasmon frequency should match the radiation frequency. This means that the bandgap energy of semiconductor $E_{gap}$ should match the surface plasmon energy, e.g. $E_{gap}=\hbar\omega_{sp}$. Thus, by obtaining the surface plasmon frequency $\omega_{sp}$ enables further investigation of the characteristics of the surface plasmons at metal-dielectric interface.

The details of the derivation of the surface plasmon dispersion follow the treatment in reference [7]. By solving Maxwell's equations, one obtains the dispersion equation as follow

$$K_{sp}=\frac{\omega}{c}\sqrt{\frac{\varepsilon_m'\varepsilon_d}{\varepsilon_m'+\varepsilon_d}}+i\frac{\omega}{c}\left(\frac{\varepsilon_m'\varepsilon_d}{\varepsilon_m'+\varepsilon_d}\right)^{\frac{3}{2}}\frac{\varepsilon_m''}{2\varepsilon_m'^2} \tag{2.1}$$

where $\varepsilon_m=\varepsilon_m'+\varepsilon_m''$ is the metal relative permittivity, $\varepsilon_d$ is the relative permittivity of the dielectric material, $\frac{\omega}{c}$ is the wave vector of the propagating wave in vacuum. The first term of Eq. (2.1) is surface plasmon dispersion, and the second term corresponding to the damping factor of SP mode. If we assume a low damping factor, which lies in the loss term, and the Drude model reduces to $\varepsilon_d=1-\frac{\omega_p^2}{\omega^2}$, where $\omega_p$ is the regular plasma frequency.

The expression for the surface plasmon frequency can be derived by substituting the equation of relative permittivity of dielectric into the dispersion relation and letting $\omega=\omega_{sp}$. Take the limit of $K_{sp}$ to $\infty$, and we get the surface plasmon frequency,

$$\omega_{sp}=\sqrt{\frac{\omega_p}{1+\varepsilon_m}} \tag{2.2}$$

Thus, the surface plasmon frequency is analogous to the regular plasma frequency, and according to Eq. (2.2), one can obtain the surface plasmon frequency below the plasma frequency $\omega_p$.

The dispersion relation is plotted in Fig. 2-3. The dash line of surface plasmon frequency is going horizontal along the propagation constant $k_x$. There is no SPP modes above the line of SP, and for the light line, just regular waves exist to the left of this line, and to the right they're cut off. So the SPP modes only exist within the shaded region.
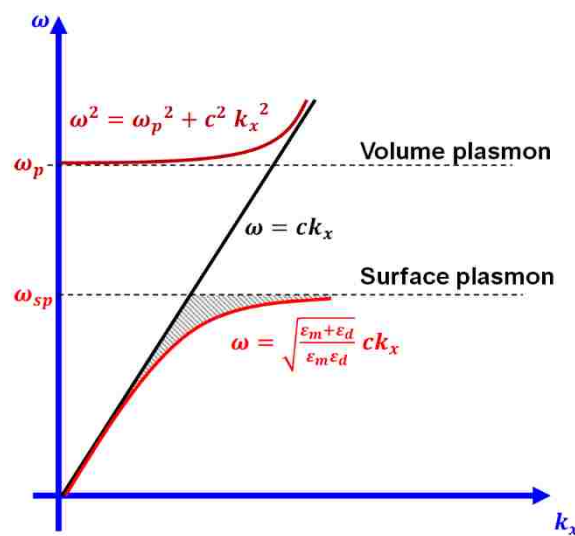


**Figure 0-3.** Dispersion relation of a SPP.

## 2.2. Loss from Metal

Surface plasmon is attracting much attention in the optics area for its useful propagation characteristics and highly subwavelength. However, the charge density wave moves back and forth and will cause very strong absorption or scattering at particular frequencies, thus it suffers from extraordinary losses from the metal. In an unpatterned metal-dielectric layer structure, the dispersion diagram of SPP lies below

13

the light line, so that such a dissipation of the photon energy dominantly comes from Ohmic loss in metal.

Attributing to the metal dissipation loss, the SP coupling technique can be used only for the devices of intrinsically low emission efficiency. In the LED application, the SP coupling technique is useful for enhancing the efficiency of InGaN-based LED, which usually has lower internal quantum efficiency. The use of metal nanostructure engineering can be designed to minimize the metal loss.

## 2.3. Surface Plasmon Effect on Spontaneous Emission Rate

It has been well known that the environment surrounding an excited atom can alter its spontaneous emission (SE) rate, and the enhancement of SE in a resonant cavity was first predicted by Purcell [8]. Purcell effect is the enhancement of the spontaneous emission rate of the fluorescent molecule by its environment, and the density of final states can be changed by modifying the surrounding environment of an emitter. Due to Purcell effect, when the $\omega_{sp}$ of Ag overlaps with the emission frequency of the InGaN QWs, the energy coupled to the SP will notably increase and hence the internal quantum efficiency (IQE) will be enhanced.

For the conventional uncoated InGaN QWs structure, both radiative and non-radiative recombination need to be taken into account, which are described by the recombination rate $\Gamma_0(\omega)$ and $\Gamma_{nr}(\omega)$, respectively. For the QWs structure coated with metal film, a new spontaneous emission channel is introduced into surface plasmons, hence the total recombination rate becomes $\Gamma_p(\omega)+\Gamma_0(\omega)+\Gamma_{nr}(\omega)$. The ratio

14

which is the analog of the Purcell factor $F_p(\omega)$ can be expressed as follow

$$F_p(\omega)=\frac{\Gamma_p(\omega)+\Gamma_0(\omega)+\Gamma_{nr}(\omega)}{\Gamma_0(\omega)+\Gamma_{nr}(\omega)}\approx 1+\frac{\Gamma_p(\omega)}{\Gamma_0(\omega)} \tag{2.3}$$

According to the Fermi's golden rule,

$$\Gamma_p(\omega)=\frac{2\pi}{\hbar}|\langle f|H|i\rangle|^2 * \rho(\hbar\omega) \tag{2.4}$$

where $\vec{d}$ represents the electron-hole pair moment, a is the location of the QW relative to the metal-dielectric interface, $\langle f|H|i\rangle$ is the matrix element of perturbations between final and initial states, and $\rho(\hbar\omega)$ is the mode density of final state. Therefore, two ways for enhancing the radiative recombination rate in QWs, namely: 1) to enhance electron and hole wavefunction overlap, and 2) to enhance the density of final state.

Figure 2-4 shows the process of spontaneous emission of the carriers in the quantum well. There are some inevitable loss channels, because metal has dissipations. In this process by using SPPs, the energy is effectively transferred from carriers in InGaN QWs into the surface plasmon for emission, which means that we alternatively create a new emission channel to enhance the photon generation rate.
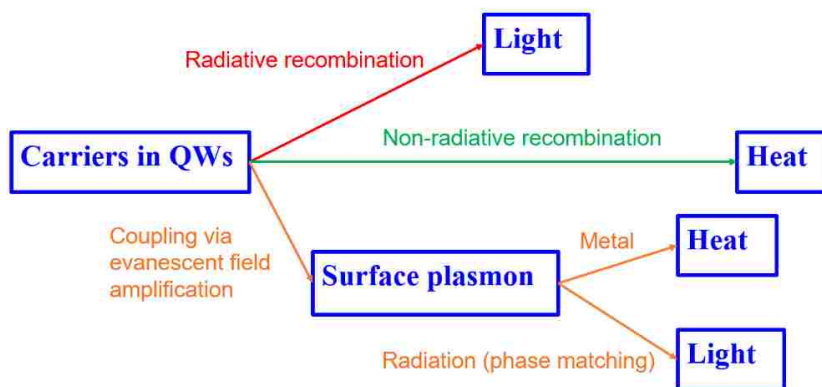


**Figure 0-4.** spontaneous emission channels of carriers in the InGaN QWs

The strong dispersive properties of SPPs allows to guide wave along the surface of a metal, which introduces new mechanisms for manipulating waves, and it is a huge area of research because of its wide range of applications: sensing application with SPR, data storage, subwavelength optics, SP-enhance Raman spectroscopy, plasmonic integrated optoelectronics, light emission/ absorption enhancement, and others. In the context of LED applications, the engineering of the surface plasmon frequency allows the optimization of the Purcell enhancement peak for achieving dramatic increase in the spontaneous emission rate in the active region of the emitters.

**References for Chapter 2**

1. Drexhage, K. H. "Interaction of light with monomolecular dye layers."*Progress in Optics* 12 (1974).

2. Ford, G. W., and W. H. Weber. "Electromagnetic interactions of molecules with metal surfaces." *Physics Reports* 113.4, 195-287 (1984).

3. Koichi Okamoto, Isamu Niki, and Axel SchererYukio Narukawa and Takashi MukaiYoichi Kawakami. "Surface plasmon enhanced spontaneous emission rate of InGaN⁄GaN quantum wells probed by time-resolved photoluminescence spectroscopy." *Applied Physics Letters*87.7, 1687 (2005).

4. Neogi, Arup, and Zhiming M. Wang. *Nanoscale Photonics and Optoelectronics: Science and Technology*. Springer (2011).

5. I. Gontijo, M. Boroditsky and E. Yablonovitch. "Coupling of InGaN quantum-well photoluminescence to silver surface plasmons." *Physical Review B* 60.60, 100 – 101 (1999).

6.    Koichi Okamoto, Isamu Niki, Alexander Shvartser, Yukio Narukawa, Takashi Mukai and Axel Scherer. "Surface-plasmon-enhanced light emitters based on InGaN quantum wells." *Nature Materials* 3.9, 601-5 (2004).

7.    Maier, Stefan Alexander. *Plasmonics: fundamentals and applications.* Springer Science & Business Media, 2007.

8.    E. M. Purcell, "Proceedings of the American Physical Society." *Phys Rev* 69.3-4, 133-133 (1946).

# Chapter 3: Theoretical Analysis of Surface Plasmon Enhancement

## 3.1. Classical Analysis

The recombination rate enhancement produced by surface plasmon polariton structures can be determined using a classical model of fluorescence near the metal surfaces, which allows computing the emission rates over the entire $k - \hbar\omega$ plane, and which has been proven quite accurate in describing a wide range. In this model, the emissive layer is treated as a plane of electric dipole sources of frequency $\omega$, of which radiated field is Fourier expanded in a sum of plane or evanescent waves over all values of the in-plane wavevector k. For all these component waves, the reflected waves from the metallic layers are calculated using a matrix technique to account for the multiple interfaces, and their amplitudes are then added [1].

We consider the emission to take the form of a forced damped harmonic oscillation. The equation of motion for the electronic dipole moment $p$ is

$$\frac{d^2 p}{dt^2} + \omega_0^2 p = \frac{e^2}{m} E_r - b_0 \frac{dp}{dt} \tag{3.1}$$

where $\omega_0$ is the resonant angular frequency in the absence of all damping, $m$ is the effective mass, $e$ is the electric charge, $E_r$ is the reflected field at the dipole position and $b_0$ is the damping constant, which corresponding to the inverse of lifetime. The reflected field does work on the dipole and they oscillate with the same complex frequency $\Omega = \omega - \frac{ib}{2}$, that is

$$p = p_0 \exp(-i\Omega t) = p_0 \exp[-(\frac{i\omega + b}{2}) t] \tag{3.2}$$

$$E_r = E_0 \exp(-i\Omega t) \tag{3.3}$$

where $\omega$ and $b$ are the frequency and damping rate respectively. Substitute Eq. (3.2) and Eq.(3.3) into Eq. (3.2), and equalize the real and imaginary components, we find that

$$\frac{b}{b_0} = 1 + \frac{e^2}{m\omega p_0 b_0} \text{Im}(E_0) \tag{3.4}$$

$$\Delta\omega \approx \frac{b^2}{8\omega} - \frac{bb_0}{4\omega} - \frac{e^2}{2m\omega_0 p_0} \text{Re}(E_0) \tag{3.5}$$

We see from equations (3.4) and (3.5) that the normalized damping rate and frequency shift are related to the out-of-phase and the in-phase components respectively of the reflected field. The change to the damping rate is dictated by the reflected field. Calculating the reflected field has been the focus of many research reports; most make use of a Green function approach, often involving an expansion of the dipole field in terms of plane waves [2]. The derivation presented here follows the treatment in reference 2. We shall not follow through the development that leads to the reflected field, we are here only interested in the result. Any dipole orientation may be considered as a combination of perpendicular and parallel dipole components. The parameters $z_\perp$ and $z_\parallel$ are given by

$$z_\perp = 1 - \frac{3}{2} \text{Im} \int_0^\infty \frac{u^3}{l_1} \left(1 - r_{1,2}^p\right) \exp(-i\beta) du \tag{3.6}$$

$$z_\parallel = 1 - \frac{3}{4} \text{Im} \int_0^\infty \frac{u}{l_1} \left[\left(1 + r_{1,2}^s\right) - (1 - u^2)\left(1 + r_{1,2}^p\right)\right] \exp(-i\beta) du \tag{3.7}$$

Several parameters need further explanation here. The integration variable $u$ is the component of the wave-vector in the plane of the interface, normalized with respect

to the far-field wave-vector of the dipole radiation field in medium 1. The parameter $l_1$ is given by $l_1 = -i * \sqrt{(1 - u^2)}$, and it is related to the component of the wave-vector perpendicular to the interface. The phase angle is the phase due to retardation, which is the phase change incurred in the round trip from the emitter, to the interface and back. The coefficients $r_{1,2}^p$ and $r_{1,2}^s$ are the Fresnel reflection coefficients for p- and s-polarized light respectively at the interface, and they're described as a function of u. And the latter may range over all positive values between 0 and infinity, the reflection coefficients have to be calculated for both real and imaginary angles of incidence. These correspond to incident waves that are propagating and evanescent respectively. We note that, when a multilayer structure capable of supporting guided modes is present, the perpendicular dipole will couple to only transverse magnetic (TM) polarized modes since $z_\perp$ involves only $r_{1,2}^p$. A dipole of any other orientation will be able to couple to transverse electric (TE) and TM modes, if present, since $z_\parallel$ contains both $r_{1,2}^p$ and $r_{1,2}^s$.

The equations (3.6) and (3.7) provide a particularly convenient formulation of the problem. The decay rates can be evaluated simply from the knowledge of the reflection coefficients of the interface between the upper half-space and the substrate. An important aspect of this technique is that it does not require us to calculate the modal properties of the structure under investigation. Further, by making straightforward modifications to Eq. (3.6) and Eq. (3.7) the system under study can be extended to include multilayers below and above the dipole, a matrix method being used to calculate the reflection coefficients for the multilayers.

Next, we assume that the dipole orientation as isotropic, by which we mean a dipole whose moment rotates and samples all directions in space in a time much faster than the fluorescence lifetime.

The spontaneous emission rate (into both radiative and SPP modes) $\Gamma$ is then computed by the dipole on the radiation field as follows,

$$\Gamma = -\frac{\omega}{2} \text{Im}(\vec{p}^* * \vec{E}) \tag{3.8}$$

where $\vec{p}$ is the dipole moment and $\vec{E}$ is the total (emitted plus reflected) field at the dipole location. This rate is finally divided by the same quantity in the absence of any metallic layers to yield the spontaneous emission rate enhancement, which is analogous to the Purcell factor. The result of this analysis depends on whether the dipoles are perpendicular or parallel to the interfaces and can be written as follows

$$F_\perp = \text{Re} \int_0^\infty \frac{3}{2} \tag{3.9}$$

## 3.2. Purcell Calculation

The localized electric field $\vec{E}(a)$ of the SP mode at the location of the QWs can be used to determine the recombination rate $\Gamma_p(\omega)$ of the spontaneous emission into the plasmon continuum in the QWs. By using Fermi's golden rule,

$$\Gamma_p(\omega) = \frac{2\pi}{\hbar} \langle \vec{d} * \vec{E}(a) \rangle^2 \rho(\hbar\omega) \tag{3.10}$$

where $\vec{E}(a)$ is normalized to a half quantum for zero-point fluctuations by the following denominator

$$E^2(a) = \frac{\hbar\omega/2}{\frac{L^2}{4\pi} \int_{-\infty}^\infty [\partial(\omega\varepsilon)/\partial\omega] E_0^2(x)\,dx} E_0^2(a) \tag{3.11}$$

where $E_0^2$ represents the unnormalized electric field, $L^2$ is the in-plane quantization

21

space, and $\hbar\omega/2$ is the energy of vacuum fluctuation [3].

For a non-dispersive medium, the integrand in equation (3.11) will be simply $\varepsilon E_0^2(x)$, however in the case of highly dispersive medium like metals, the appropriate expression to be used for the electric energy density is $[\partial(\omega\varepsilon)/\partial\omega]E_0^2(x)/8\pi$. Note that $\varepsilon$ varies in frequency and also with the vertical position in the multilayer structure.

The density of SP modes is obtained according to the other density of states calculations in solid state physics [4]. For a frequency range $d\omega$, the number of corresponding modes in the two-dimensional k space is

$$\rho(\hbar\omega) = \frac{2\pi k\, dk}{(2\pi)^2\, d(\hbar\omega)}L^2 = \frac{L^2}{4\pi}\frac{d(k^2)}{d(\hbar\omega)}$$

(3.12)

Therefore, the density of plasmon modes $\rho(\hbar\omega)$ can be obtained from the derivative $\frac{d(k^2)}{d(\hbar\omega)}$ of the dispersion relation $\omega(k)$. The recombination rate into the surface plasmon modes can be obtained by combining Eq. (3.10), Eq. (3.11) and Eq. (3.12) as following,

$$\Gamma_p(\omega) = \frac{2}{3}\frac{2\pi}{\hbar}d^2\frac{\hbar\omega/2}{\frac{L^2}{4\pi}\int_{-\infty}^{\infty}[\partial(\omega\varepsilon)/\partial\omega]E_0^2(x)\,dx}E_0^2(a)\frac{L^2}{4\pi}\frac{d(k^2)}{d(\hbar\omega)}$$

(3.13)

$$\Gamma_p(\omega) = \frac{2}{3}\frac{\pi d^2\,\omega E_0^2(a)}{\hbar\int_{-\infty}^{\infty}[\partial(\omega\varepsilon)/\partial\omega]E_0^2(x)\,dx}\frac{d(k^2)}{d(\omega)}$$

(3.14)

where the factor 2/3 comes from the ratio of the coupling strengths of dipole moment $\vec{d}$ parallel to $E_\perp$ and $E_\parallel$ for conduction band to light hole band (C-LH) transition. This plasmon recombination rate has to be compared to the spontaneous emission rate $\Gamma_0(\omega)$ in bulk semiconductors, which can be formulated using the classical formula

$$\Gamma_0(\omega) = \frac{4nd^2\,\omega^3}{3\hbar c^3}$$

(3.15)

Putting Eq. (3.14) and Eq. (3.15) into Eq. (2.3), we obtain the Purcell enhancement factor $F_p$ for the spontaneous emission into the surface plasmon modes

as

$$F_p(\omega) = 1 + \cfrac{\dfrac{2}{3} \cfrac{\pi d^2 \omega E_0^2(a)}{\hbar \int_{-\infty}^{\infty} [\partial(\omega\varepsilon)/\partial\omega] E_0^2(x)\,dx} \dfrac{d(k^2)}{d(\omega)}}{\dfrac{4nd^2\omega^3}{3\hbar c^3}} \qquad (3.16)$$

$$F_p(\omega) = 1 + \frac{\pi c^3 E_0^2(a)}{2n\omega^2 \int_{-\infty}^{\infty} [\partial(\omega\varepsilon)/\partial\omega] E_0^2(x)\,dx} \frac{d(k^2)}{d(\omega)} \qquad (3.17)$$

In the derivation above, the fact the conduction-to-heavy hole band transition (C-HH) can be treated as it couple to electric fields which is polarized in the QW plane (y-z plane). On the other hand, C-LH transitions couple twice as strongly to electric fields with polarization which is perpendicular to the x direction than to those polarized in the y-z plane In the classical spontaneous emission model, C-HH transitions are described with parallel dipoles, while C-LH transitions are described according to both parallel and perpendicular dipoles, which are weighted by a factors of 1/3 and 2/3, respectively [5].

## 3.3.  Calculation for Multilayer Structure

So far, we have calculated the surface plasmon (SP) dispersion equation for the waves propagating in the interface of two semi-infinite half-space metal and dielectric materials. The wave equation for TM modes propagating in the $+\hat{z}$ direction is given by

$$\vec{H_i} = \hat{y}\, H_i(x) \exp\left[\, j\,(\omega t - \gamma z)\, \right] \qquad (3.18)$$

$$\vec{E_i} = \left[ \hat{x}\, \frac{\gamma}{\omega\varepsilon(x)} H_i(x) + \hat{z}\, \frac{-j}{\omega\varepsilon(x)} \frac{\partial H_i(x)}{\partial x} \right] \exp\left[\, j\,(\omega t - \gamma z)\right] = \hat{r}\, E_i(x)\exp\left[j(\omega t - \gamma z)\right]$$

$$(3.19)$$

where $\gamma$ is the complex propagation constant, $\varepsilon(x) = \varepsilon_0\,\varepsilon_r(x)$ is the permittivity, and $\hat{r} = \hat{x} + \hat{z}$ represents the direction of the electric field. Moreover,

$$H_i(x) = A_i \exp\left[-k_i(x - x_{i-1})\right] + B_i \exp\left[k_i(x - x_{i-1})\right] \tag{3.20}$$

is the y-component of the magnetic field amplitude of the wave propagating in the $i^{th}$ layer and $k_i = \sqrt{\gamma^2 - \frac{\omega^2}{c^2} n_i^2}$ is the normal component of wavevector (in the $\hat{x}$ direction). $A_i$ and $B_i$ complex coefficients refers to $+\hat{x}$ and $-\hat{x}$ propagating wave respectively and $x_i$ indicates the boundary between the $i^{th}$ and $(i+1)^{th}$ layer. TM boundary conditions require that tangential field components e.g. $H_i(x)$ and $\frac{1}{n^2}\frac{dH_i(x)}{dx}$ continuous across the interfaces between the layers. Therefore, in the $i^{th}$ layer,

$$H_i(x) = A_i \exp\left[-k_i(x - x_{i-1})\right] + B_i \exp\left[k_i(x - x_{i-1})\right] \tag{3.21}$$

$$\frac{1}{n^2}\frac{dH_i(x)}{dx} = \frac{1}{n_i^2}\left[k_i(-A_i \exp[-k_i(x-x_{i-1})] + B_i \exp[k_i(x-x_{i-1})])\right] \tag{3.22}$$

and in the $(i+1)^{th}$ layer,

$$H_{i+1}(x) = A_{i+1}\exp[-k_{i+1}(x-x_i)] + B_{i+1}\exp[k_{i+1}(x-x_i)] \tag{3.23}$$

$$\frac{1}{n^2}\frac{dH_{i+1}(x)}{dx} = \frac{1}{n_{i+1}^2}\left[k_{i+1}(-A_{i+1}\exp[-k_{i+1}(x-x_i)] + B_{i+1}\exp[k_{i+1}(x-x_i)])\right]$$

$$\tag{3.24}$$

At the interface between the $i^{th}$ and $(i+1)^{th}$ layer, i.e. at $x = x_i$, the values of the Eq. (3.21) and Eq. (3.23) are equal and give the following

$$A_i \exp[-k_i\,d_i] + B_i \exp[k_i\,d_i] = A_{i+1} + B_{i+1} \tag{3.25}$$

where $d_i$ is the thickness of the $i^{th}$ layer. Similarly, the values of Eq. (3.22) and (3.24) are also equal at $x = x_i$ and they give the following equation,

$$\frac{1}{n_i^2}[k_i(-A_i \exp[-k_i\,d_i] + B_i \exp[k_i\,d_i])] = \frac{1}{n_{i+1}^2}[k_{i+1}(-A_{i+1} + B_{i+1})] \tag{3.26}$$

24

The equations (3.25) and (3.26) can be manipulated to give expressions for $A_{i+1}$ and $B_{i+1}$ as follow

$$A_{i+1} = \frac{1}{2}\left[A_i\left(1 + \frac{n_{i+1}^2}{n_i^2}\frac{k_i}{k_{i+1}}\exp[-k_i d_i]\right) + B_i\left(1 - \frac{n_{i+1}^2}{n_i^2}\frac{k_i}{k_{i+1}}\exp[k_i d_i]\right)\right] \qquad (3.27)$$

$$B_{i+1} = \frac{1}{2}\left[A_i\left(1 - \frac{n_{i+1}^2}{n_i^2}\frac{k_i}{k_{i+1}}\exp[-k_i d_i]\right) + B_i\left(1 + \frac{n_{i+1}^2}{n_i^2}\frac{k_i}{k_{i+1}}\exp[k_i d_i]\right)\right] \qquad (3.28)$$

The equations above can be put into matrix form as

$$\begin{pmatrix} A_{i+1} \\ B_{i+1} \end{pmatrix} = Q_i \begin{pmatrix} A_i \\ B_i \end{pmatrix} \qquad (3.29)$$

where the transfer matrix of the i$^{th}$ layer, $Q_i$ is given by

$$Q_i = \frac{1}{2}\begin{pmatrix} \left[1 + f_i\frac{k_i}{k_{i+1}}\right]\exp[-k_i d_i] & \left[1 + f_i\frac{k_i}{k_{i+1}}\right]\exp[-k_i d_i] \\ \left[1 + f_i\frac{k_i}{k_{i+1}}\right]\exp[-k_i d_i] & \left[1 + f_i\frac{k_i}{k_{i+1}}\right]\exp[-k_i d_i] \end{pmatrix} \qquad (3.30)$$

For the case of TE modes, $f_i = 1$ and for TM modes, $f_i = \frac{n_{i+1}^2}{n_i^2}$. The transfer matrix $Q_i$ relates the complex field coefficients at the interface between the i$^{th}$ and (i-1)$^{th}$ layer and for a multi-layer waveguide with l layers, the transfer matrix of the whole waveguide is given by

$$Q_{wg} = \prod_{i=l-1}^{0} Q_i \qquad (3.31)$$

and relates the field coefficients in the cover and the substrate layer, i.e.

$$\begin{pmatrix} A_c \\ B_c \end{pmatrix} = Q_{wg}\begin{pmatrix} A_s \\ B_s \end{pmatrix} \qquad (3.32)$$

where the elements of the transfer matrix are denoted as

$$Q_{wg} = \begin{pmatrix} q_{11} & q_{12} \\ q_{21} & q_{22} \end{pmatrix} \qquad (3.33)$$

## 3.4. Rigorous Method for Dispersion Calculation

The relation between the incident, reflection, and the transmission for the

multilayered structures is given by

$$\begin{pmatrix} A_l \\ 0 \end{pmatrix} = \begin{pmatrix} q_{11} & q_{12} \\ q_{21} & q_{22} \end{pmatrix} \begin{pmatrix} 1 \\ B_0 \end{pmatrix} \tag{3.34}$$

Since the magnetic field for TM modes in the output medium propagates in a single direction only, the sign of k must be chosen appropriately. In this case where we have substrate illumination, the magnetic field in the cover layer propagates in the $+\hat{x}$ direction, i.e., $\text{Im}[k_c > 0]$ and $B_c = 0$. The reflection coefficient is

$$R = \frac{B_0}{A_0} = -\frac{q_{21}}{q_{22}} \tag{3.35}$$

The reflection coefficient (R) is a function of the complex propagation constant $\gamma$. The guided or leaky modes correspond to the resonances of the layered waveguide structure, which happen at the poles of the reflection coefficient R. According to (3.35), the poles of the reflection coefficient are solutions of $q_{22}(\gamma)=0$.

We know that the obtained dispersion equation is a complex function of $\omega$ and $\gamma$, which should be solved. In order to find the roots of a complex function, we must have both real and imaginary parts of the function equals to zero. So, we have a nonlinear equation set as following that should be solved

$$\begin{cases} \text{Re}[q(\gamma)]=0 \\ \text{Im}[q(\gamma)]=0 \end{cases} \tag{3.36}$$

where $\gamma$ is the complex propagation constant, which indicates the modes (both guided and leaky one).

To find the roots of the complex equation $q_{22}(\gamma)=0$ is numerically challenging. Reflection pole method (RPM) examines the RPM phase as a function of the real part of the propagation constant [6]. Based on the Bode-plot theory (but with frequency on the real axis), for the case of modes with no loss, the RPM phase response

26

is a summation of the step functions where the number of steps equals to the number of

guided modes, and the height of each step is exactly π. Each π step is located at a $\beta$

which is equal to the real part of propagation constant of the lossless guided modes.

For the case of a lossy or leaky guided mode, there is an abrupt variation in the RPM

phase of the magnitude which is in the vicinity of the $\beta$ corresponding to the

propagation constant [7].

The resulting spectrum of a single mode has the Lorentzian-type peak at $\beta$ and

has a half width at half maximum (HWHM) equal to α, where it corresponds to the

complex propagation constant of the lossy guided or leaky mode of the multilayer

structure.

We can approximate the denominator of the reflection coefficient as an $N^{th}$

degree polynomial. In order to find the analytic expression of the quantity $d\varphi_{RPM}/d\beta$

we must collect all the coefficients of Eq. (3.36) with the same power of $\beta$. For example,

for a fifth-degree polynomial, of which the coefficients are

$$r_4 = -(\gamma_1 + \gamma_2 + \gamma_3 + \gamma_4 + \gamma_5)$$
$$r_3 = \gamma_1\gamma_2 + \gamma_1\gamma_3 + \gamma_1\gamma_4 + \gamma_1\gamma_5 + \gamma_2\gamma_3 + \gamma_2\gamma_4 + \gamma_2\gamma_5 + \gamma_3\gamma_4 + \gamma_3\gamma_5 + \gamma_4\gamma_5$$
$$r_2 = $$
$$-(\gamma_1\gamma_2\gamma_3 + \gamma_1\gamma_2\gamma_4 + \gamma_1\gamma_2\gamma_5 + \gamma_1\gamma_3\gamma_4 + \gamma_1\gamma_3\gamma_5 + \gamma_1\gamma_4\gamma_5 + \gamma_2\gamma_3\gamma_4 + \gamma_2\gamma_3\gamma_5 + \gamma_2\gamma_4\gamma_5 + \gamma_3\gamma_4\gamma_5)$$
$$r_1 = \gamma_1\gamma_2\gamma_3\gamma_4 + \gamma_1\gamma_2\gamma_3\gamma_5 + \gamma_1\gamma_2\gamma_4\gamma_5 + \gamma_1\gamma_3\gamma_4\gamma_5 + \gamma_2\gamma_3\gamma_4\gamma_5$$
$$r_0 = -\gamma_1\gamma_2\gamma_3\gamma_4\gamma_5$$

$$(3.37)$$

Using Eq. (3.37), the phase of the reflection coefficient denominator $q_{22}(\beta)$ can be

obtained analytically as follow

$$\varphi_{RPM} = \tan^{-1}\left(\frac{\text{Im}[q_{22}(\beta)]}{\text{Re}[q_{22}(\beta)]}\right) \tag{3.38}$$

and the derivative of the phase of $q_{22}(\beta)$ with respect to $\beta$ is

$$\frac{d}{d\beta}\varphi_{RPM}=\frac{\mathrm{Re}[q_{22}(\beta)]^2}{\mathrm{Re}[q_{22}(\beta)]^2+\mathrm{Im}[q_{22}(\beta)]^2}\times\frac{\mathrm{Re}[q_{22}(\beta)]\frac{d}{d\beta}\mathrm{Im}[q_{22}(\beta)]-\mathrm{Im}[q_{22}(\beta)]\frac{d}{d\beta}\mathrm{Re}[q_{22}(\beta)]}{\mathrm{Re}[q_{22}(\beta)]^2}$$

(3.39)

## 3.5. Field Distribution

After solving the dispersion equation, we still need to know the complex

coefficients, $A_i$ and $B_{il}$, to find the field distribution profile. As we know the field

must decay down in both cladding and substrate layers. Thus from Eq. (3.34), we have

$$\begin{pmatrix}A_l\\0\end{pmatrix}=\begin{pmatrix}q_{11}&q_{12}\\q_{21}&q_{22}\end{pmatrix}\begin{pmatrix}0\\B_0\end{pmatrix}$$

(3.40)

which yields to

$$A_l=q_{12}B_0$$

(3.41)

The equation (3.41) is an equation with two variables. Thus, we need one more equation,

to find an unique solution for that. The other equation comes from the normalization of

the filed such that the field carries 1 Watt of power flow along the $\hat{z}$ axis per unit width

in the $\hat{y}$ direction. Thus, we have

$$\frac{1}{2}\int_{-\infty}^{\infty}H_y E_x^* dx=\frac{1}{2}\int_{-\infty}^{\infty}H_i(x)\frac{\gamma^*}{\omega\varepsilon^*(x)}H_i^*(x)\,dx=\frac{\gamma^*}{2\omega}\int_{-\infty}^{\infty}\frac{|H_i(x)|^2}{\varepsilon^*(x)}\,dx=1$$

(3.42)

or using $\varepsilon(x)=\varepsilon_0\varepsilon_r(x)$, we get

$$\int_{-\infty}^{\infty}\frac{|H_i(x)|^2}{\varepsilon_r^*(x)}\,dx=\frac{2\omega\varepsilon_0}{\gamma^*}$$

(3.43)

In order to calculate the integration, we need $|H_i(x)|^2$ which is given by

$$|H_i(x)|^2=H_i(x)H_i^*(x)$$
$$=(A_i\exp[-k_i(x-x_{i-1})]+B_i\exp[k_i(x-x_{i-1})])(A_i\exp[-k_i(x-x_{i-1})]+B_i\exp[k_i(x-x_{i-1})])^*$$
$$=\begin{cases}|A_i|^2\exp[-(x-x_{i-1})(k_i+k_i^*)]+|B_i|^2\exp[(x-x_{i-1})(k_i+k_i^*)]\\+A_iB_i^*\exp[-(x-x_{i-1})(k_i-k_i^*)]+B_iA_i^*\exp[(x-x_{i-1})(k_i-k_i^*)]\end{cases}$$

28

$$(3.44)$$

And the integration gives

$$\frac{|B_0|^2}{(k_0+k_0^*)\varepsilon_{r0}^*}+\frac{|A_l|^2}{(k_l+k_l^*)\varepsilon_{rl}^*}+\sum_{j=1}^{l-1}\frac{1}{\varepsilon_{rj}^*}\left[\begin{array}{l}\dfrac{|A_j|^2}{(k_j+k_j^*)}\left(\exp\left[-d_j(k_j+k_j^*)\right]-1\right)+\dfrac{|B_j|^2}{(k_j+k_j^*)}\left(\exp\left[d_j(k_j+k_j^*)\right]-1\right)\\[3mm]+\dfrac{A_jB_j^*}{(k_j-k_j^*)}\left(\exp\left[-d_j(k_j-k_j^*)\right]-1\right)+\dfrac{B_jA_j^*}{(k_j-k_j^*)}\left(\exp\left[d_j(k_j-k_j^*)\right]-1\right)\end{array}\right]$$

$$=\frac{2\omega\varepsilon_0}{\gamma^*}$$

$$(3.45)$$

where the coefficients inside the summation are related to $B_0$ and $A_1$ by Eq. (3.29).

Thus we find the second equation that we need to find $B_0$ and $A_1$. After getting $B_0$

and $A_1$, we can find the complex field coefficients of intermediate layers by using Eq.

(3.29).

The plasmon wave guided modes correspond to the rapid changes of the phase

of $q_{22}(\gamma)$. According to Bode plot theory, a peak of the derivative of the phase of

$q_{22}(\gamma)$ corresponds to the real part index of a guided mode, and the full width at half

maximum of the phase derivative curve is the imaginary part of mode index [8].

The electromagnetic field of a mode with a particular k-vector can be described

as follow

$$\vec{E}(\vec{r},t)=\frac{1}{2}\left[D\vec{f}_{\vec{k}}(\vec{r})\eta(t)+cc\right]\qquad(3.46)$$

$$\vec{H}(\vec{r},t)=\frac{1}{2}\frac{1}{\mu_0}\left[\frac{D}{\omega_{\vec{k}}}\nabla\times\vec{f}_{\vec{k}}(\vec{r})\chi(t)+cc\right]\qquad(3.47)$$

with $\eta(t)=q(t)+ip(t)$, and $\chi(t)=p(t)-iq(t)$. Here, $q(t)\equiv-\cos(\omega_k t)$ and

$p(t)\equiv-\sin(\omega_k t)$ describe time-varying (oscillating) parts, $\mu_0$ is the magnetic

permeability of free space, and $D$ is a constant. $\vec{f}_{\vec{k}}(\vec{r})$ is a normalized time-

independent part of electric field: $\vec{f}_{\vec{k}}(\vec{r}) = \vec{u}_{\vec{k}}(z)e^{i\vec{k}.\vec{x}}$ with $\iiint \partial(\varepsilon\omega)/\partial\omega|\vec{u}_{\vec{k}}|^2 \, d\vec{r} = 1$. The total energy can then be expressed as

$$W = \frac{1}{2}\iiint [\partial(\varepsilon\omega)/\partial\omega\vec{E}(\vec{r},t)^2 + \mu_0\vec{H}(\vec{r},t)^2]d\vec{r} = \frac{1}{2}D^2\frac{1+\Theta_k}{2}(p^2+q^2) \quad (3.48)$$

where $1/(1 + \Theta_{\vec{k}})$ describes the ratio of the electric field energy to the total field energy ($\Theta_{\vec{k}} = \iiint(1/\mu_0)\left|\nabla\times(\vec{f}_{\vec{k}}/i\omega_{\vec{k}})\right|^2 d\vec{r}$). The choice of $D = -i\sqrt{2\omega_{\vec{k}}/(1 + \Theta_{\vec{k}})}$ satisfies Hamilton's equations: $-\partial W/\partial p = \omega_{\vec{k}}p = \dot{q}$, and $-\partial W/\partial q = \omega_{\vec{k}}q = \dot{p}$.

Then the mode can be represented aas a harmonic oscillator, the Hamiltonian quantized, and the electric field operator expressed as

$$\vec{E}(\vec{r},t) = i\sqrt{\frac{\hbar\omega_{\vec{k}}}{1+\Theta_{\vec{k}}}}\vec{f}_{\vec{k}}(\vec{r})a + H.C. \quad (3.49)$$

where $H.C.$ is the hermitian conjugate. In a dielectric structure $1/(1 + \Theta_{\vec{k}})$ equals 1/2. However, in a plasmonic structure (a structure with metal), the introduction of the $1/(1 + \Theta_{\vec{k}})$ term is critical, as the energy is not equally distributed between the electric and magnetic fields. At the metal-dielectric boundaries, the oscillation of the magnetic field induces surface charges because of the discontinuity of the conductivity on metal surface. The distribution of these charges produces an electric field $\vec{E}_k$ parallel to the metal surface by Coulomb's law. At a frequency close to the SPP's resonant frequency $\nu_{sp}$, high density of the surface charges induces a large $\vec{E}_k$ around the metal-dielectric boundary. This field-charge interaction increases $1/(1 + \Theta_{\vec{k}})$ from 1/2, storing more energy in the electric field than in the magnetic field.

The SE rate $\Gamma$ for the exciton lying in the vicinity of a metal surface is enhanced from the SE rate $n\Gamma_0$ in a dielectric with index n due to the Purcell

enhancement effect. Here, $\Gamma_0$ is the SE rate for the exciton lying in vacuum. To analyze the SE rate enhancement for the exciton with a radiative frequency $\nu$ coupled to traveling SPPs, the Purcell enhancement factor $F(\nu)$, defined as the $\Gamma$ normalized by $n\Gamma_0$, has been studied. In this definition, we ignore the nonradiative decay of the exciton. As opposed to Purcell factor for the exciton coupled to a resonant cavity, $F(\nu)$ represents the electrodynamics of the exciton coupled to a number of traveling SPP modes. In a uniform metal surface, the SPP frequency $\omega$ is almost independent of its propagation constant $k$ at the resonant frequency $\nu_{sp} \equiv \omega_p/\sqrt{1 + n^2}$, where $\omega_p$ is the regular plasma frequency of the metal. This k-independence of $\omega$ increases the density of SPP states $D(\omega)$ and supports a large number of SPPs which are coupled to excitons at $\nu_{sp}$. While this increase of $D(\omega)$ contributes to the part of the $\Gamma$ enhancement, the field confinement of the SPP at the metal-dielectric interface also contributes to the Purcell effect. The field confinement of SPP increases the photon energy density (PED), and enhances the coupling effect of excitons near the metal surface and SPP modes which is relative to the coupling between the same excitons and non-SPP modes. The dissipation of the photon energy from each SPP mode has an additional effect on $\Gamma$. It gives the SE into each SPP mode a spectral width, analogous to Purcell effect in a cavity. In an unpatterned metal-dielectric layer structure, the dispersion diagram of SPP lies below the light line, so that such a dissipation of the photon energy mainly comes from the ohmic loss in metal. For investigation of $F(\nu)$ in this part, we consider the mechanisms above according to quasi-quantum electrodynamics (QED) analysis [9].

Here, the theoretical formulation of $F(\nu)$ for the exciton lies in the vicinity of

a uniform metal-dielectric interface. Including the effect of the ohmic loss in the metal,

we assume a dissipative SPP mode with the following time evolution of its E-field,

$$\vec{E}_{\vec{k}}(\vec{r},t)=\vec{E}_{\vec{k}}(\vec{r})\times\exp\{-i(\omega_{\vec{k}}-i\,\omega_{\vec{k}}/Q_{\vec{k}})t\} \tag{3.50}$$

where $\omega_{\vec{k}}$ and $Q_{\vec{k}}$ are the frequency and the quality factor of k-mode, respectively.

For simplicity, we take the SPP-related part $F^{sp}(v)$ as defined by $F^{sp}(v) \equiv \Gamma^{sp}/n\Gamma_0$,

where $\Gamma^{sp}$ is the SE rate into SPP modes. $F(v)$ is obtained by summing $F^{sp}(v)$ and

the non-SPP-related part $F^{non-sp}(v)$: $F(v) = F^{sp}(v) + F^{non-sp}(v)$. By solving the

Jaynes-Cummings Hamiltonian with the multimode field expressed by Eq. (3.50),

$$F^{sp}(v)=\sum_{\vec{k}} \frac{2\pi}{n\Gamma_0(v)}\left|g_{\vec{k}}(d)\right|^2 D_{\vec{k}}(v) \tag{3.51}$$

$$D_{\vec{k}}(v) = \frac{1}{\pi}\frac{\omega_{\vec{k}}/2Q_{\vec{k}}}{\left(\omega_{\vec{k}}-v\right)^2+\left(\omega_{\vec{k}}/2Q_{\vec{k}}\right)^2} \tag{3.52}$$

where $g_{\vec{k}}(d)$ is the coupling strength between k-mode and the exciton located at $z=d$

defined as $g_{\vec{k}}=g_0\Psi(z)\cos(\xi)$, where $g_0=\frac{\mu}{\hbar}\sqrt{\frac{\hbar v}{(1+\Theta_{\vec{k}})\varepsilon V_{\vec{k}}}}\frac{\mu}{\hbar}\sqrt{\frac{\hbar v}{2\varepsilon V_{\vec{k}}}}$, $\Psi(z)=\frac{\left|\vec{E}_{\vec{k}}(z)\right|}{\max\left|\vec{E}_{\vec{k}}(z)\right|}$, and

$\cos(\xi) = \vec{e}_{\vec{k}}\cdot\vec{e}_{\vec{\mu}}$. Here, $V_{\vec{k}}$ is the SPP mode volume, and $\vec{e}_{\vec{k}}$ and $\vec{e}_{\vec{\mu}}$ are unit vectors for

the SPP electric field and the electric field dipole $\vec{\mu}$, respectively. $D_{\vec{k}}(v)$ shown in Eq.

(3.52) gives the Lorentzian spectrum for the SE into K-mode. The density of the SPP

states does not show up in Eq. (3.51). However, $\sum_{\vec{k}} D_{\vec{k}}(v)$ becomes the density of the

SPP states in case $D_{\vec{k}}(v) \rightarrow \delta(\omega_{\vec{k}} - v)$ with $Q_{\vec{k}} \rightarrow \infty$. To investigate the enhanced

SE rate into each k-mode, we introduce the distributed Purcell factor which defined by

the following

$$F^{sp-dis}(v,\vec{k})\equiv\frac{1}{\Delta k^x\Delta k^y}\frac{2\pi}{n\Gamma_0(v)}\left|g_{\vec{k}}(d)\right|^2 D_{\vec{k}}(v) \tag{3.53}$$

where $\Delta k^x \Delta k^y \equiv (2\pi)^2/l^2$ is the reciprocal space of an SPP mode. If the real-space area $l^2$ is large enough, then k can be considered as continuous. Eq. (3.53) is rewritten as $F^{sp-dis}(v, \vec{k}) = \partial^2 F^{sp}(v)/\partial k^x \partial k^y$. In that case, the SE rate into a small reciprocal area $\Delta_{\vec{k}}$, normalized by $n\Gamma_0$, is expressed as $F^{sp-dis}(v, \vec{k})\Delta_{\vec{k}}$. The mode volume for each travelling SPP mode is expressed as $V_{\vec{k}} = l^2 L_{\vec{k}}$, where $L_{\vec{k}}$ is defined as the 1D integral of the PED [9],

$$L_{\vec{k}} = \frac{\int \{\partial(\omega\varepsilon)/\partial\omega\}_{\omega=v} |\vec{E}_{\vec{k}}(z)|^2 dz}{\max\left[\{\partial(\omega\varepsilon)/\partial\omega\}_{\omega=v} |\vec{E}_{\vec{k}}(z)|^2\right]} \tag{3.54}$$

By combining Eq. (2.45) and (2.46), $F^{sp-dis}(v, \vec{k})$ is rewritten as follows

$$F^{sp\text{-}dis}(v,\vec{k}) = \frac{3}{2} \frac{1}{n^3} \frac{c^3}{v^2} \frac{H_{\vec{k}}(d)}{L_{\vec{k}}} \frac{1}{1+\Theta_{\vec{k}}} (\vec{e}_{\vec{k}} \cdot \vec{e}_{\vec{\mu}}) D_{\vec{k}}(v) \tag{3.55}$$

where

$$H_{\vec{k}}(z) = \frac{\varepsilon_{\omega=v} |\vec{E}_{\vec{k}}(z)|^2}{\max\left[\{\partial(\omega\varepsilon)/\partial\omega\}_{\omega=v} |\vec{E}_{\vec{k}}(z)|^2\right]} \tag{3.56}$$

At a uniform metal-dielectric interface, $\omega_{\vec{k}}$, $Q_{\vec{k}}$, and $L_{\vec{k}}$ are independent of the direction of $\vec{k}$. By rewriting Eq. (3.51) as the integral in the polar coordinates $\vec{k} = (k, \varphi)$, $F^{sp}(v)$ can be expressed as a function of the propagation constant $k = |\vec{k}|$ below the light line

$$F^{sp}(v) = \int_{k_0(v)}^{\infty} F_{uniform}^{sp\text{-}dis}(v, k) dk \tag{3.57}$$

where $k_0(v)$ is $k$ on the light line. $F_{uniform}^{sp-dis}(v, k)$ is the integral of $F^{sp-dis}(v, \vec{k})$ over $\varphi$

$$F_{uniform}^{sp\text{-}dis}(v,k) \equiv \int_0^{2\pi} k F^{sp\text{-}dis}(v,\vec{k}) d\varphi = \frac{3\pi}{n^3} \frac{c^3}{v^2} \frac{1}{1+\Theta_{\vec{k}}} \cdot \frac{h_k(d)}{L_k} \cdot k D_k(v) \tag{3.58}$$

Here, $h_k(z)$ is defined as an integral of $1/2\pi \cdot H_{\vec{k}}(d) \cdot (\vec{e}_{\vec{\mu}} \cdot \vec{e}_{\vec{k}})^2$ over $\varphi$

33

$$h_k(z) = \alpha \frac{\varepsilon_{\omega=\nu} \left| \vec{E}_k^i(z) \right|^2}{\max \left[ \{ \partial(\omega\varepsilon)/\partial\omega \}_{\omega=\nu} \left| \vec{E}_k(z) \right|^2 \right]} \tag{3.59}$$

where $\alpha = 1/2$ and $\vec{E}_k^i(z) = \vec{E}_k^z(z)$ when the dipole moment of the emitter $\vec{\mu}$ is in the plane of the metal surface, and $\alpha = 1$ and $\vec{E}_k^i(z) = \vec{E}_k^z(z)$ when $\vec{\mu}$ is out of the plane.

## References for Chapter 3

1.  Paiella, Roberto. "Tunable surface plasmons in coupled metallo-dielectric multiple layers for light-emission efficiency enhancement." *Applied Physics Letters* 87.11, 111104 (2005).

2.  Chance, R. R., A. Prock, and R. Silbey. "Lifetime of an emitting molecule near a partially reflecting surface." *The Journal of Chemical Physics* 60.7, 2744-2748 (1974).

3.  Barnes, W. L. "Fluorescence near interfaces: the role of photonic mode density." *Journal of modern optics* 45.4, 661-699 (1998).

4.  Gontijo, I., et al. "Coupling of InGaN quantum-well photoluminescence to silver surface plasmons." *Physical Review* B 60.16, 11564 (1999).

5.  Vuckovic, Jelena, Marko Loncar, and Axel Scherer. "Surface plasmon enhanced light-emitting diode." *IEEE Journal of Quantum Electronics* 36.10, 1131-1144 (2000).

6.  Guo, Junpeng, and Ronen Adato. "Extended long range plasmon waves in finite thickness metal film and layered dielectric materials." *Optics express* 14.25 12409-12418 (2006).

7. Anemogiannis, Emmanuel, Elias N. Glytsis, and Thomas K. Gaylord. "Determination of guided and leaky modes in lossless and lossy planar multilayer optical waveguides: reflection pole method and wavevector density method." *Journal of lightwave technology* 17.5, 929 (1999).

8. Guo, Junpeng, and Ronen Adato. "Extended long range plasmon waves in finite thickness metal film and layered dielectric materials." *Optics express* 14.25, 12409-12418 (2006).

9. Neogi, Arup, and Zhiming M. Wang. *Nanoscale Photonics and Optoelectronics: Science and Technology*, Springer (2011).

# Chapter 4: Simulation of Surface Plasmon Dispersion Engineering

## 4.1. Material Properties

In this work, the pursuit of suitable plasmonic materials for enhancing the efficiency of InGaN QW LEDs in the range of long-wavelength emission is pursued. Here we want to find applicable and appropriate metal combinations to couple with InGaN/GaN QW in long-wavelength.

It has been known from Drude-Lorentz model that there is the oscillation of electrons and metals when there exists a surface wave. In order to include the contributions of interband and intraband transitions, we use the Drude-Lorentz model to explore the SP characteristics of some metal candidates.

The free electron response in metals can be described as Eq. (4.1)

$$\varepsilon(\omega) = \varepsilon_{\infty} - \frac{\omega_p{}^2}{\omega^2 - i\Gamma_D\omega} + \sum_{j=1}^{m} \frac{f_j * \omega_{oj}{}^2}{\omega_{oj}{}^2 - \omega^2 + i\gamma_j\omega} \qquad (4.1)$$

The first term $\varepsilon_{\infty}$ is the background dielectric constant, and it is included in the equation because the contributions of higher energy level transition are not taken into account by the Lorentz term. The second term refers to the Drude term, which is described by plasma frequency $\omega_p$ and the damping factor $\Gamma_D$. The third term includes each of the Lorentz oscillators which is at the location of the energy position $E_{oj} = \hbar\omega_{oj}$ with the strength $f_j$ and the damping factor $\gamma_j$. Optical constants of some metal materials are obtained from [1]-[2], and the values of Drude-Lorentz model parameters are given in Table 4-1.

**Table 0-1.** Values of the Drude-Lorentz model parameters for Au, Ag, Al and TiN

|  | Au | Ag | Al | TiN |
|---|---|---|---|---|
| $\varepsilon_\infty$ | 9.1 | 3.7 | 7 | 1.95 |
| $\hbar\omega_p$ (eV) | 9.03 | 9.01 | 14.98 | 1.009 |
| $\Gamma_D$ | 0.053 | 0.048 | 0.047 | 0.118 |
| $f_1$ | 0.024 | 0.065 | 0.227 | 0.18 |
| $\gamma_1$ | 0.241 | 3.886 | 0.333 | 0.023 |
| $\hbar\omega_{o1}$ (eV) | 0.415 | 0.816 | 0.162 | 0.553 |
| $f_2$ | 0.01 | 0.124 | 0.05 | 6.88 |
| $\gamma_2$ | 0.345 | 0.452 | 0.312 | 0.148 |
| $\hbar\omega_{o2}$ (eV) | 0.83 | 4.481 | 1.544 | 0.92 |

We assume that the plasmonic material has infinite thickness, so we use the infinite half-space to engineer the dispersion relation of plasmonic materials. An infinite half-space is a region in space that is bounded at only one edge, and it extends to infinity in the direction away from the interface. By using the assumption of the material thicknesses extending to infinity on both sides, there cannot be any contributing waves out extending to infinity. The field decays exponentially, away from the interface, and it is free to propagate without decay in the plane of the interface.

We simulate the surface plasmon dispersion such that different materials have

been investigated to find the appropriate candidate for long-wavelength emission. Some

of the metals such as Au, Ag, Al, ad TiN have been explored, and the simulation results
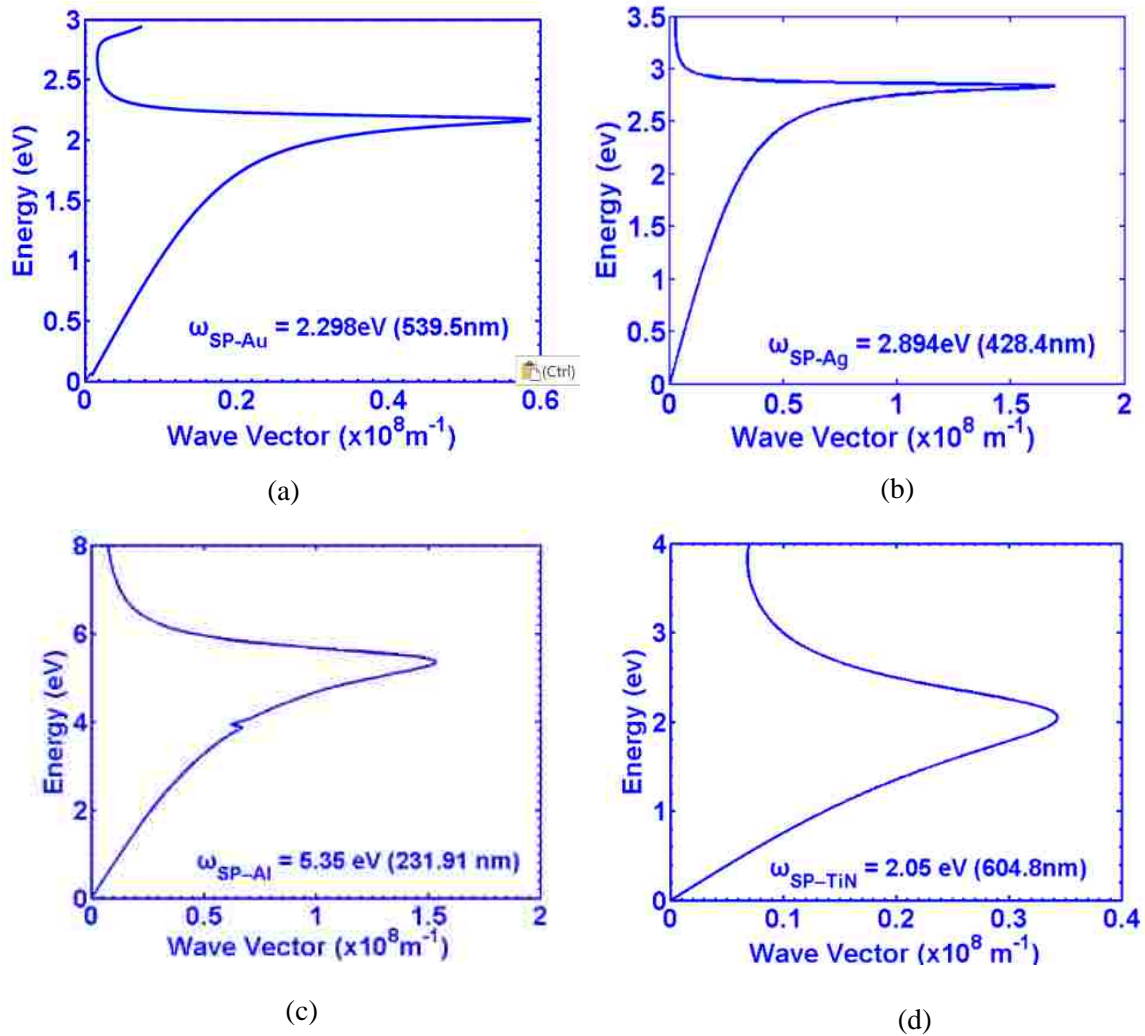
for their dispersion relation are shown in Fig 4-1.



**Figure 0-1.** Surface plasmon dispersion relation of (a) Au, (b) Ag, (c) Al, and (d) TiN in semi-infinite space

As can be seen from Fig. 4-1, Au has a surface plasmon frequency $\omega_{sp}$ of 2.29eV

(539.5nm), Ag has a $\omega_{sp}$ of 2.894eV (428.4nm), Al has a $\omega_{sp}$ of 5.35eV (231.91nm), and

TiN has a $\omega_{sp}$ of 2.05eV (604.8nm) when they are deposited on top of GaN. Thus, the

Ag and Al are obviously not good candidates for implementation in the InGaN/GaN

LED emitting in the long-wavelength regime. However, we find that the surface

plasmon frequency of Au lies in the green spectra regime, and for TiN, the surface plasmon frequency matches the amber emission. Thus, the implementation of the Au and TiN for green and amber LEDs, respectively, is feasible. Thus, the optimization of the SP dispersion in the long wavelength regime will implement the TiN and combination of the TiN / Au.

## 4.2. Single Metallic Layer Model

We use Au and TiN to enhance the radiation efficiency of InGaN QW at long-wavelengths through surface plasmon, and the enhancement of efficiency in the LED is based on Purcell effect. Here the spacer separation between metallic layer and QWs is set to 10nm. We choose 10nm GaN spacer thickness, and investigate the Purcell enhancement factor of different thicknesses of metal layer. Figure 4-2 and Figure 4-3 show the computational results of dispersion relation and Purcell factor for Au and TiN.
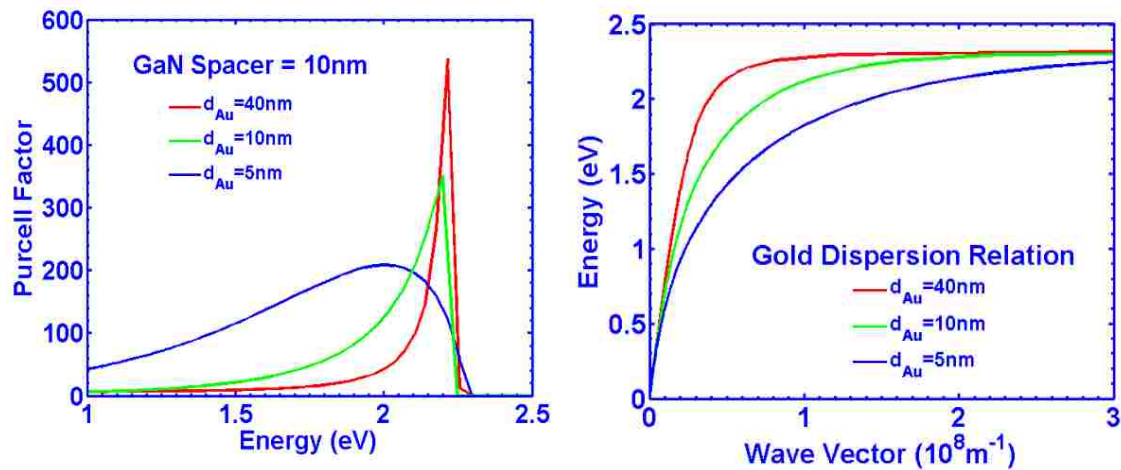


**Figure 0-2.** Purcell factor (left) and dispersion relation (right) of Au deposited on top of GaN spacer = 10nm, with Au thickness = 40nm, 10nm, 5nm, respectively.
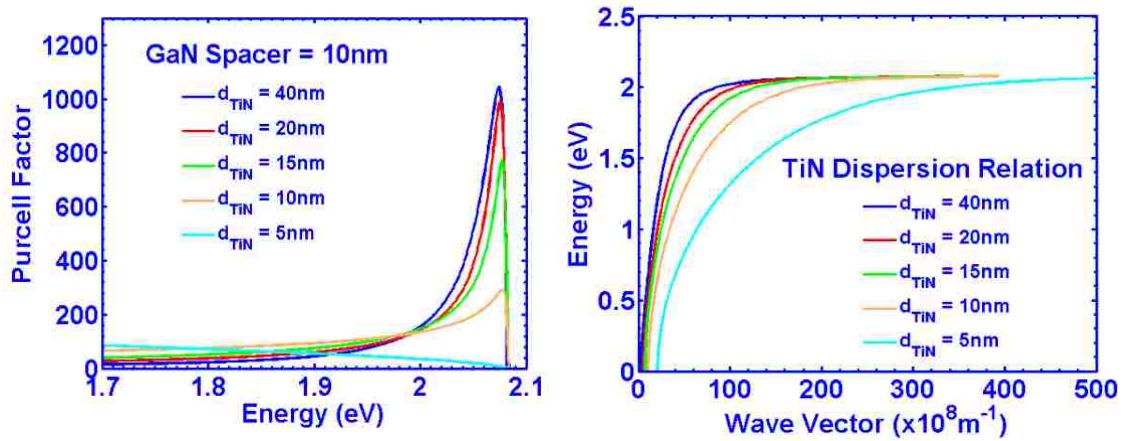
**Figure 0-3.** Purcell factor (left) and dispersion relation (right) of TiN deposited on top of GaN spacer = 10nm, with TiN thickness = 40nm, 20nm, 15nm, 10nm, 5nm, respectively.

The simulation results show that the Purcell factor is decreasing when the thickness of Au and TiN reduces. For the largest enhancement results, Au has the Purcell factor of ~500 times in the green spectrum, and TiN could provide the excellent performance for surface plasmon dispersive property in the amber region with the Purcell factor of ~1000 times.

Using single metallic layer leads to strong enhancement in $R_{Rad}$ near the $\omega_{sp}$, however the enhancement will reduce down for frequency further away from the $\omega_{sp}$ such that no enhancement obtained for frequency above $\omega_{sp}$. This phenomenon of the use of single SP metallic layer coupled QWs had been demonstrated to result in an order-magnitude of enhancement in the green-emitting InGaN QWs through PL measurement in many reports [3].

## 4.3. Double Metallic Layers Model

As our design is intended to tune the surface plasmon frequency within the range of long-wavelength emission, the use of single metallic will not provide the tunability

40

capability. In 2011, H. Zhao, et al. reported that double metallic layers provided the frequency tunability functionality in the optimum Purcell enhancement factor in appropriate operating frequency [3]. Here, we propose to use the double metallic layers model to control the surface plasmon dispersion, and we use the double layer models of TiN / Au and Au/ TiN with target operating wavelength near the red emission regime. The schematics of TiN / Au and Au/ TiN double metallic layers structures are shown in Figure 4-4.
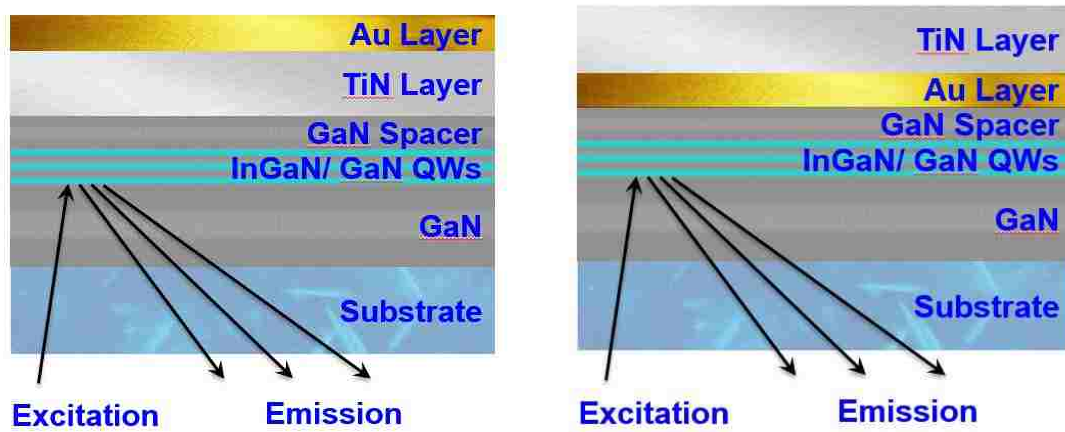


**Figure 0-4.** Schematic of double metallic layers of TiN/Au (left) and Au/ TiN (right) on top of GaN

The spacer separation between metallic layer and QW is set to 10nm. We choose the GaN spacer thickness of 10nm, and use different thicknesses of TiN and Au layers, of which the total metallic thickness remains the same as 40nm. The simulation results of the double metallic layers model of TiN/Au have been provided as follows.
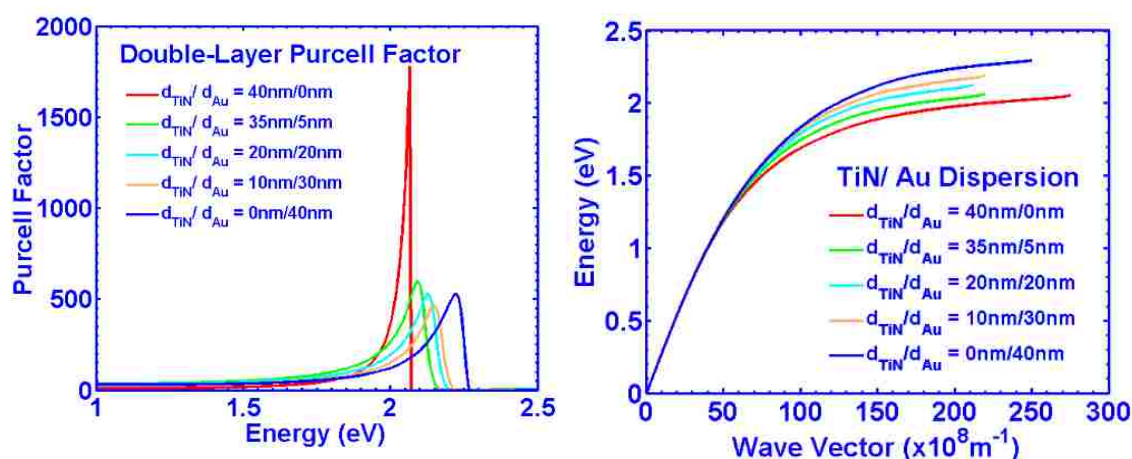
41

**Figure 0-5.** Purcell factor (left) and dispersion relation (right)of TiN/Au double metallic layers deposited on top of GaN spacer = 10nm, with $d_{TiN}/d_{Au}$ = 40nm/0nm, 35nm/5nm, 20nm/20nm, 10nm/30nm, 0nm/40nm, respectively.

As shown in the simulation results (figure 4-5), the use of TiN / Au double metallic layer enables the tuning of surface plasmon frequency in the wavelength regime of interest – namely in the range of 539 nm up to 604 nm [figure 4-5(b)]. Thus, the use of TiN / Au double metallic layer structure can be considered an applicable method to tune of surface plasmon dispersion between the SP frequencies of TiN and Au.

Moreover, besides of the tunability, it was found that TiN / Au double metallic layers placed over the InGaN QWs can be tuned to provide an increase in the Purcell enhancement factor in the long-wavelength spectra regime by ~500 times [figure 4-5(a)], which indicates it can also provide the high enhancement tuning in the wavelength of interest where the InGaN QWs active region has low IQE.

We also apply Au/ TiN double layers model to understand about its enhancement effect. The simulation results are shown in figure 4-6. From the results in Fig. 4-6, the use of Au/ TiN also exhibits both the tunability within the range of surface plasmon frequency of Au and TiN, and the enhancement of coupling into InGaN QWs. But the enhancement of this structure is ~200 times, which is not as strong as that of TiN / Au double layer due to weaker coupling effect. The use of Au-layer as the first layer reduces the plasmonic effect introduced by the TiN layer attributed to the weak field interaction with the plasmon layer.
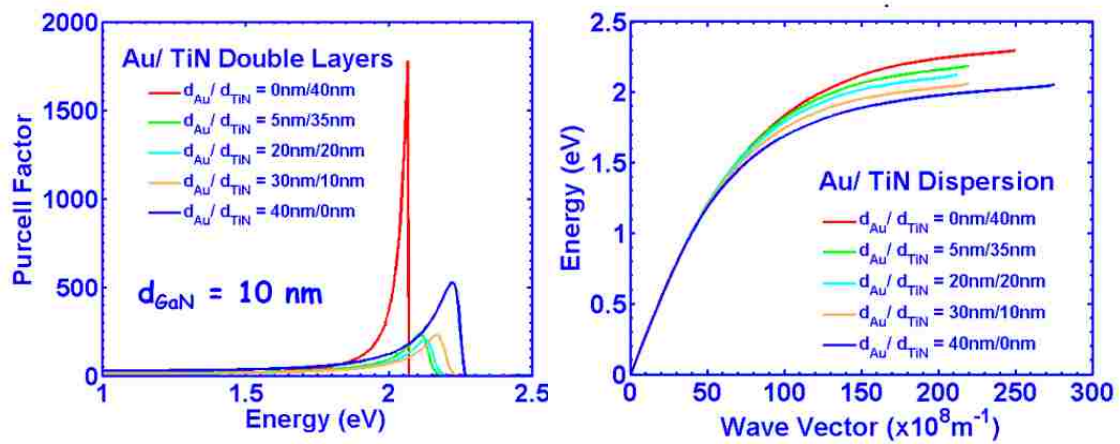


**Figure 0-6.** Purcell factor (left) and dispersion relation (right)of Au/TiN double metallic layers deposited on top of GaN spacer = 10nm, with dAu/dTiN = 0nm/40nm, 5nm/35nm, 20nm/20nm, 30nm/10nm, 40nm/0nm, respectively.

## 4.4. Energy Shift

Based on the simulation results of the TiN/ Au and Au/ TiN structure above, there exists a minor energy shift of surface plasmon. These comparisons are plotted in figure 4.7. As shown in Fig. 4-7, for 35nm TiN/ 5nm Au structure, the SP frequency is smaller as compared to that of the 5nm TiN/ 35nm Au. Thus, the deposition of TiN as the first layer in the double metallic design results in stronger red shift in the SP

frequency of the structure. The order of the metallic layer plays significant role in determining the interaction strength between the field with the plasmonic layer, thus it is essential for one to design the TiN as the first layer in the studied structure for long wavelength emitter application.
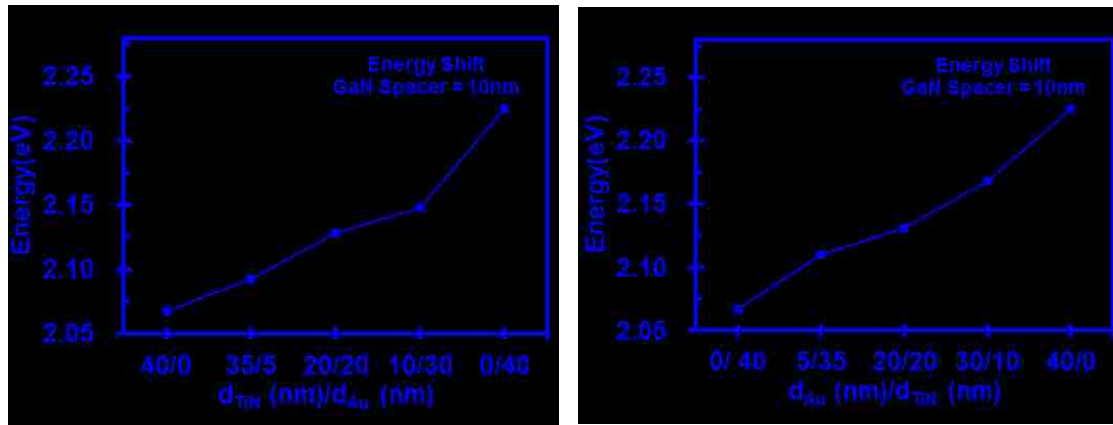


**Figure 0-7.** Energy shift of double metallic layer of TiN/ Au (left) and Au/ TiN (right)

## 4.5.    Effect of Different Spacer Thickness on Purcell Enhancement

The density of states at the location of the InGaN QWs relative to the metal-dielectric interface will influence the coupling effect between metal layer and GaN. Thus, we investigate various GaN spacer thickness to change the relative location of QWs to explore the coupling effect of QWs and metallic layers. We choose to use GaN spacer thickness of 4nm and 15nm respectively, with TiN/ Au double layers structure as simulated before. The Purcell factor enhancement for the case with different spacer thicknesses is shown in Fig. 4-8.
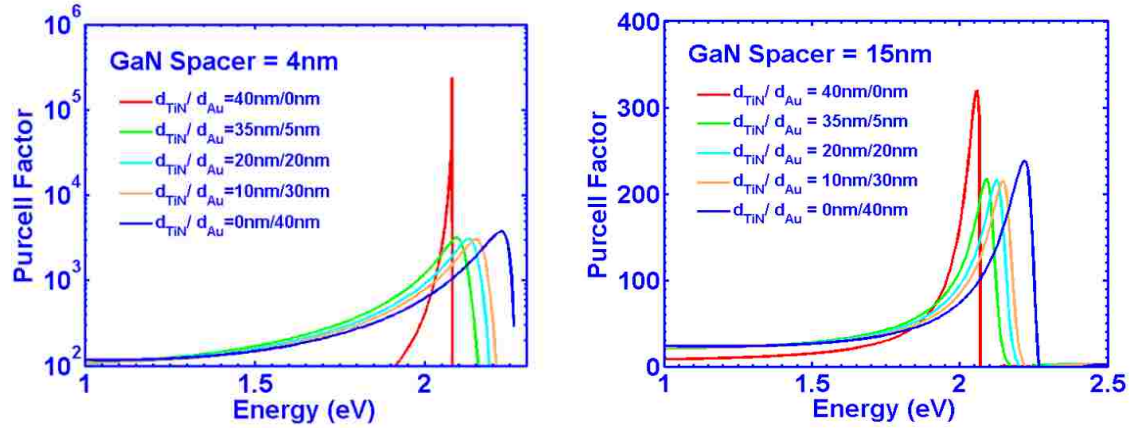
**Figure 0-8.** Purcell factor of TiN/ Au double layers with 4nm GaN spacer (left) and 15nm GaN spacer (right)

As shown in figure 4-8, there is decreasing Purcell factor enhancement for an increasing GaN spacer thickness. By comparing this result with the previous data of ~500 times of enhancement with 10nm GaN spacer (in Fig. 4-5), the use of 4nm GaN spacer [Fig. 4-8(a)] results in a large increase of Purcell enhancement factor ~ 1000. In contrast, the use of 15nm spacer [Fig. 4-8(b)] results in a reduction in the Purcell factor of only 200 times. Attributing to the weaker coupling between SP and QWs, the increase of GaN spacer separation leads to the smaller Purcell enhancement factor.

And from the simulation above, we notice that the SP frequency for the peak of Purcell factor of different GaN spacer has a small change, although it is not obvious with these value configurations of thickness. Thus, the effect of different spacer thickness with 40nm TiN single layer is investigated.
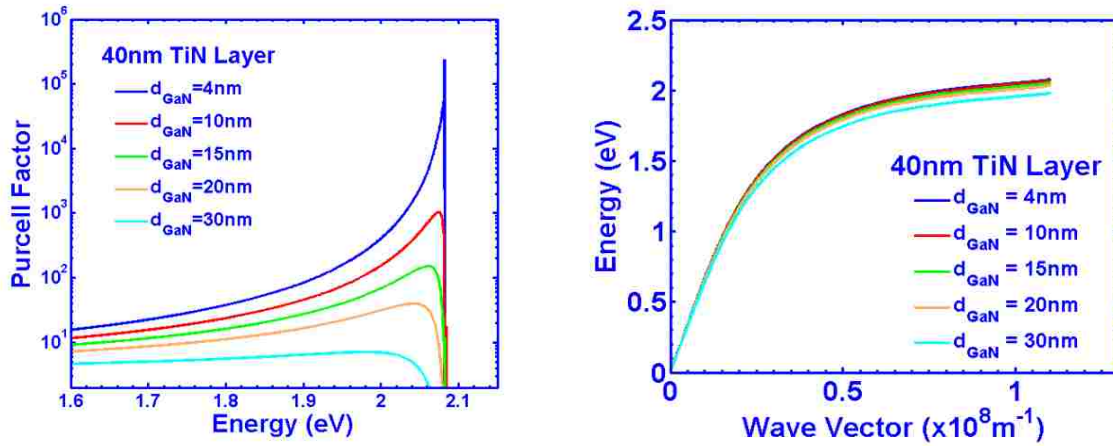
**Figure 0-9.** Purcell factor (left) and dispersion relation (right) of 40nm TiN single metallic layer deposited on top of GaN spacer = 4nm, 10nm, 15nm, 20nm, 30nm , respectively

Based on the results in Fig. 4-9, the dispersion relation shows there exists a slight energy shift of SP frequency for variation of spacer thickness in the 40-nm thick TiN layer structure. For the Purcell effect, the result shows a larger enhancement factor with the smaller GaN spacer separation, which matches the trend of that of double-layer model.

Based on the simulation in this chapter, in order to optimize a SP coupled QWs structure, we have to consider the number of metallic layers, the thickness of metallic layer, and the separation of spacer, which will affect the enhancement and emission range of surface plasmon frequency. With an optimized SP structure, a strong enhancement is obtained as the energy coupled to the SP is increasing and thus internal quantum efficiency will be enhanced.

**References for Chapter 4**

1.  Aleksandar D. Rakić, Aleksandra B. Djurišić, JM Elazar and ML Majewski. "Optical properties of metallic films for vertical-cavity optoelectronic devices." *Applied Optics*37.22, 5271-5283 (1998).

2.  Patsalas, Panos, Nikolaos Kalfagiannis, and Spyros Kassavetis. "Optical properties and plasmonic performance of titanium nitride." *Materials* 8.6, 3128-3154(2015).

3.  Hongping Zhao, Jing Zhang, Guangyu Liu, and Nelson Tansu. "Surface plasmon dispersion engineering via double-metallic Au/Ag layers for III-nitride based light-emitting diodes." *Applied Physics Letters* 98.15, 236 (2011).

# Chapter 5: Summary and Future Work

The objective of this thesis is to use surface plasmon (SP) coupling to the InGaN/ GaN QWs to enhance the radiation efficiency of LED. The use of SP has been proven and demonstrated both theoretically and experimentally that SP can provide a notable enhancement of internal quantum efficiency (IQE). Using surface plasmon dispersion engineering is a method of creating a new emission channel to amplify the light generation rate, and it can effectively transfer the energy from carriers in InGaN/ Gan QWs into the surface plasmon mode attributed to the higher density of state which in turn results in faster photon generation rate. When the surface plasmon frequency of metal material overlaps with the emission frequency of the InGaN QWs, the energy coupled to the SP will greatly increase and thus IQE will be strongly enhanced.

In order to achieve the desirable long-wavelength emission and enhance the radiation efficiency, the plasmonic properties of some metal materials have been explored to design the SP structure on top of GaN spacer. TiN and Au have been selected as appropriate plasmonic material to couple to the InGaN/ GaN QWs and hence enhance their efficiency through surface plasmons. The simulation results of the dispersive properties show that TiN with $\omega_{sp}$ of 2.05 eV (605nm) could be a good candidate for amber emission; meanwhile the $\omega_{sp}$ of Au lies in 2.298 eV (539.5nm) matches the green emission. It has been simulated that the Purcell factor of Au is of ~550 times, and the Purcell factor of TiN is of ~1000 times in the green and amber spectral regimes, respectively, which demonstrates its applicability for this structure for IQE enhancement in those respective LEDs. However, the limitation for the single

metallic layer is that it can only be used in the specific emission spectrum, and cannot be tuned at the other frequency away from the SP frequency for the enhancement will decay very fast in the other spectral region.

For the double metallic layers of TiN/ Au, the simulation shows both the flexible tuning capability by changing the thickness of metallic layers, which enables a large Purcell enhancement factor in the range of SP frequencies between those of Au and TiN (green-amber). The Purcell enhancement for double-layer model reduces as compared to those of single metallic layer, however the its large tunability provides the practical ability for designing this structure for specific emitters – specifically for addressing the red emission spectral regime.

For future work, some experiments can be designed to investigate and demonstrate the dispersive characteristics and mechanisms of SP coupled InGaN/ GaN QWs LED. The objective of the experiments is to investigate the effect of (1) different configurations of the metallic layer and GaN spacer, and (2) In composition on $In_xGa_{1-x}N$/ GaN heterostructures on the properties and performance of LEDs. And there are some important aspects in coupling radiation to SP which should be considered, such as the exact emission spectrum of the LED, the voltage-current characteristic of the LED, and the internal efficiency without metallic layers should be known too.

For the experiment set up, the metallic layer should be sputtered through the sputtering system under the certain condition. After sputtering the metallic film on top of the LED with optimized and proper thickness, the efficiency enhancement of the LED can be tested by photoluminescence (PL) measurements. PL would be performed

by exciting the QWs with a suitable diode laser from the bottom of the substrate based on the set up shown in Figure 4-4. The ratio of the integrated photoluminescence spectra from the uncoated and metal-coated samples can be used as a direct measurement of the recombination rate enhancement.

The advantages of SP coupling can be applied in wide fields of applications for its internal quantum efficiency enhancement, light extraction improvement, reduction of efficiency droop effect. Recently Eu-doped GaN QWs has been utilized to enable red emitting GaN LED [1]. The TiN for SP single metallic layer structure, as a good material for its strong Purcell factor in the amber-red spectral regime, can be proposed to be an excellent method of enhancing the internal quantum efficiency.

**References for Chapter 5**

1.　　Fujiwara, Yasufumi, and Volkmar Dierolf. "Present understanding of Eu luminescent centers in Eu-doped GaN grown by organometallic vapor phase epitaxy." *Japanese Journal of Applied Physics* 53.5S1, 05FA13(2014).

# Curriculum Vitae

**(Ms.) Yiming Zhong**

**Cell Phone:** (610) 653-2615          **Email:** yiz515@lehigh.edu
**Address:** 430 Montclair Ave, Bethlehem, PA, 18015, USA
**Birth day:** February 10th 1993, Beijing, China & Chinese

## Education

**Lehigh University (Bethlehem, Pennsylvania, USA)          September 2015 – present**
Master of Science in Electrical Engineering, Department of Electrical and Computer Engineering

- Expected Graduation: May 2017

- Research Assistant (Center for Photonics and Nanoelectronics, Lehigh)

- Advisor: Prof. Nelson Tansu

**Nanjing University (Nanjing, Jiangsu Province, China)    September 2011 – July 2015**
Bachelor of Science in Microelectronics, Department of Electronic Science and Engineering

- Thesis: "The Reliability Research of GaN-based LED with Integrated Sensor"

- Graduate with Best Thesis Award

## Skills

**Program Design**     C programming, PSpice, OriginLab, Xilinx ISE, Verilog HDL, Multisim

**Related Courses**    Physics of Semiconductor Devices, Semiconductor Lasers, Wireless Communication, Power Electronics, Advanced E &M, Advanced Circuits, Physics of Solids, Lightwave Technology

## Professional Experiences

**Lehigh University (Bethlehem, Pennsylvania, USA)          September 2015 – present**
**Master Candidate and Research Assistant**
Center for Photonics and Nanoelectronics (CPN)
Advisor: Prof. Nelson Tansu
Project: Surface Plasmon Dispersion Engineering for Long-Wavelength Spectral Emitters

51

- Conduct the theoretical work and simulation of the dispersion relation of proper material candidates for surface plasmon

- Simulate the field distribution profile with multiple metallic layers

- Analyze the Purcell enhancement and evaluate the internal quantum efficiency of LED

- Design the optimized structure to enhance the IQE of red light emitters

**Nanjing University (Nanjing, Jiangsu Province, China)        June 2014 – July 2015**
**Undergraduate Research Assistant**
Key Lab of New Energy and Materials Engineering
Advisor: Prof. Yugang Zhou
Project: The Reliability Research of GaN-based LED with Integrated Sensor

- Analyze the physical failure mechanisms in the degradation process

- Achieve the goal of real-time online measurement

- Observe and compare correlation of photoelectric characterization of LED chip under different current stress degradation condition

- Make the evaluation of the overall reliability of the LED chip with integrated sensor to increase its reliability optimization

# Referred Conference Paper

1) I. Fragkos, C. K. Tan, **Y. Zhong**, V. Dierolf, Y. Fujiwara, and N. Tansu, "Understanding the Current Injection Efficiency in Rare-Earth Doped GaN:Eu Red-Emitting Light Emitting Diodes", Proc. of the IEEE Lester Eastman Conference on High Performance Devices 2016, Bethlehem, PA, August 2016.
2) I. Fragkos, C. K. Tan, **Y. Zhong**, V. Dierolf, Y. Fujiwara, and N. Tansu, "The role of Injection Efficiency in Eudoped GaN LED", Proc. of the MRS Fall Meeting, Rare Earths in Advanced Photonics and Spintronics, Boston, MA, November 2016.
3) **Y. Zhong**, I. Fragkos, and N. Tansu, "Surface Plasmon Dispersion Engineering by Using TiN / Au Double Metallic Layers for Yellow up to Red Spectral Emitters", Proc. of the SPIE Photonics West 2017, Photonic and Phononic Properties of Engineered Nanostructures VII, San Francisco, CA, February 2017.
4) I. Fragkos, **Y. Zhong**, C. K. Tan, V. Dierolf, Y. Fujiwara, and N. Tansu, "Enhancement of Internal Quantum Efficiency of GaN:Eu based Red Light Emitters through Surface Plasmon Engineering", Proc. of the SPIE Photonics West 2017, Light-

Emitting Diodes: Materials, Devices, and Applications for Solid State Lighting XXI, San Francisco, CA, February 2017.

5) I. Fragkos, C. K. Tan, **Y. Zhong**, V. Dierolf, Y. Fujiwara, and N. Tansu, "On the identification and understanding of limiting factors in IQE of GaN:Eu based PIN diodes for red light emission", Proc. of the SPIE Photonics West 2017, Physics and Simulation of Optoelectronic Devices XXV, San Francisco, CA, February 2017.

## Work Experience

**Internship in State Grid Corporation of China**        **June 2014 - August 2014**

Project: A Novel Hardware Implementation of SM2 Algorithm on Processor CK803

- Perform the experiment and evaluate the performance of the hardware platform;

- Simplify the original complex protocol sending between software and hardware;

- Finish function of server and checksum of the project;

**Internship in Beijing Institute of Science and Technology Information**

**June 2013 – Sep. 2013**

Project: Information Search& Analysis Through the Novel Developing Search Engine

- Use the novel search engine to analyze the data

- Compare the features of traditional search engine and novel search engine which is available to make a wide range of effective search and analysis of big data base.

- Understand the significance of developing a high-efficiency search engine;

## Honors and Awards

- The Outstanding Leader of Student Senate (2014, 2015)

- Distinction in National Undergraduate Electronics Design Contest (2014)

# References

**Prof. Nelson Tansu** [Fellow of National Academy of Inventors]
Daniel E. '39 and Patricia M. Smith Endowed Chair Professor
Smith Family Endowed Director, Center for Photonics and Nanoelectronics (CPN)
Department of Electrical and Computer Engineering (ECE)
Lehigh University
7 Asa Drive, Bethlehem, Pennsylvania 18015, USA
Email: Tansu@Lehigh.Edu, Phone: (610) 758-2678, Fax: (610) 758-2605
Research Group: www.ece.lehigh.edu/~tansu
CPN Web: www.lehigh.edu/cpn


**Prof. Jonathan J. Wierer, Jr.** (IEEE Senior Member)
Associate Professor Center for Photonics and Nanoelectronics (CPN)
Department of Electrical and Computer Engineering (ECE)
Lehigh University
7 Asa Drive, Bethlehem, PA 18015, USA
Email: jwierer@Lehigh.Edu, Phone: (610) 758-2602
CPN Web: http://www.lehigh.edu/~incpn/people/faculty/wierer.html